

# Deciphering culprits for cyanobacterial blooms and lake vulnerability in north-temperate lakes

Jacob Serpico<sup>1,a</sup>, B. A. Zambrano-Luna<sup>1,a</sup>, Russell Milne<sup>1,a</sup>, Christopher M. Heggerud<sup>2</sup>, Alan Hastings<sup>2</sup>, and Hao Wang<sup>1,\*</sup>

<sup>1</sup>Interdisciplinary Lab for Mathematical Ecology and Epidemiology & Department of Mathematical and Statistical Sciences, University of Alberta, Edmonton, Alberta T6G 2R3, Canada

<sup>2</sup>Department of Environmental Science and Policy, University of California - Davis, California 95616, United States

<sup>a</sup>These authors contributed equally to this work.

\*Corresponding author: hao8@ualberta.ca

## Abstract

Harmful cyanobacterial blooms (CBs) have a growing global prevalence, emerging as a significant environmental concern due to their potential toxicity. Understanding how the different mechanisms affect CBs is crucial to develop actionable management strategies. For this, we derive a stoichiometric dynamical system that describes the qualitative population dynamics of cyanobacteria and their toxicity in north-temperate freshwater ecosystems. Our model quantifies the hypoxic effects of CBs on fish mortality and the effect of microcystin-LR (MC-LR), a potent toxin produced by cyanobacteria, on aquatic macro-invertebrates, phytoplankton, and fish species. By fitting the model to lakes with varying physical characteristics, eutrophic conditions, and water temperature, we can delineate and understand the driving components of CBs. We show that decreases in water exchange rate, depth of epilimnion, or light attenuation increases bloom intensity and duration. Furthermore, our models concur that eutrophication and increasing water temperatures exacerbate the intensity of CBs. We observe a severe bioaccumulative effect of MC-LR in aquatic species, stressing the potential impact on humans and other terrestrial animals. We validate our model with field measurements demonstrating its applicability to several realistic lake conditions. These insights are essential for informing targeted interventions to reduce CBs and their ecological impacts.

## Author Contributions

**Jacob Serpico:** Methodology, Software, Validation, Formal analysis, Investigation, Data Curation, Writing - Original Draft, Writing - Review & Editing, Visualization, and Project administration. **B. A. Zambrano-Luna:** Methodology, Software, Validation, Formal analysis, Investigation, Data Curation, Writing - Original Draft, and Visualization. **Russell Milne:** Conceptualization, Methodology, Data Curation, Supervision, Writing - Original Draft, Writing - Review and Editing, Funding acquisition. **Christopher M. Heggerud:** Validation, Writing - Original Draft, Writing - Review & Editing. **Alan Hastings:** Validation. **Hao Wang:** Conceptualization, Methodology, Supervision, Funding acquisition.

## Competing Interests

There are no competing interests.

## Keywords

cyanobacteria, mathematical modelling, aquatic ecology, climate change, ecotoxicology

## 34 Introduction

35 In recent years, harmful cyanobacterial blooms (CBs)  
36 have become an increasing concern in lakes worldwide [1,  
37 2]. These blooms significantly impact aquatic ecosystems  
38 and human health due to the toxic chemicals, namely  
39 cyanotoxins, that cyanobacteria regularly produce. Cyan-  
40 otoxins are known to cause adverse health effects in fish  
41 that ingest them [3], livestock that drink contaminated  
42 water [4], and humans that consume affected species [5].  
43 The decomposition of dead cyanobacteria following a  
44 bloom can also deplete oxygen in lakes, further exacer-  
45 bating the environmental impact of CBs [6, 7]. Due to  
46 the multitude of harmful effects that CBs have on lake  
47 ecosystems, recent work has been conducted to identify  
48 their causative factors and forecast them ahead of time  
49 [8–10]. However, predictive models that explicitly in-  
50 corporate the effects of cyanobacterial toxins on higher  
51 trophic levels and other components of lake food webs  
52 still need to be explored [11–13].

53 Factors that influence CBs are many and diverse.  
54 Water temperature, for instance, is highly important for  
55 determining the growth of cyanobacteria [14, 15] because  
56 peak cyanobacterial growth rates occur at water temper-  
57 atures higher than what is typically observed in nature  
58 [16]. Climate change is forecast to raise lake water tem-  
59 peratures, thus creating a more favourable environment  
60 for higher cyanobacterial growth rates [17, 18]. The  
61 growth of cyanobacteria and the prevalence of CBs are  
62 strongly correlated to nutrient availability and sunlight  
63 exposure [1, 2]. Furthermore, CBs are influenced by  
64 many additional biotic and abiotic factors, such as anthro-  
65 pogenic nutrient pollution, water clarity, and temperature  
66 [9, 19]. As with temperature, increased phosphorus input  
67 from agricultural or industrial sources can exacerbate  
68 CBs [20]. These factors necessitate a comprehensive  
69 understanding of how future temperature and nutrient  
70 loading patterns may impact cyanobacterial prevalence in  
71 aquatic ecosystems, especially in lakes already threatened  
72 by cyanobacteria.

73 CBs have a multifaceted negative influence on lake  
74 ecosystems, including producing cyanotoxins and de-  
75 pleting oxygen levels. Microcystins, the most common  
76 cyanotoxins, have garnered widespread attention due to  
77 their various toxic effects on a broad range of species [21–  
78 24]. *Microcystis aeruginosa* is a freshwater cyanobacteria  
79 species responsible for the dominant production of mi-  
80 crocystins [1]. Furthermore, significant microcystin-LR  
81 (MC-LR) concentrations are readily observed in lakes  
82 following CBs, highlighting the urgency of this environ-

83 mental challenge [6, 9, 25]. The detrimental effects of  
84 MC-LR on fish health, including liver and muscle damage,  
85 have been well-documented, with implications for both  
86 aquatic ecosystems and human health [26–29]. Existing  
87 literature suggests a strong bioaccumulative effect of MC-  
88 LR and other cyanotoxins [25, 30], highlighting the threat  
89 of CBs to humans and other terrestrial or aquatic species.

90 In this study, we develop a comprehensive and ver-  
91 satile model that considers the interactions between  
92 cyanobacteria, sunlight, and nutrients (specifically phos-  
93 phorus) in a lake ecosystem; a schematic of our model  
94 is shown in Figure 1. We additionally consider the  
95 *sander vitreus* (walleye) and *perca flavescens* (yellow  
96 perch) populations, representing piscivorous (predator)  
97 and omnivorous (prey) fish species, respectively. Lastly,  
98 we consider daphnia (representing zooplankton) and al-  
99 gae (representing unicellular phytoplankton that do not  
100 produce toxins), the dynamics of dissolved oxygen, the  
101 production of toxins (namely MC-LR) by cyanobacteria,  
102 and the uptake of toxins by each aforementioned species.  
103 We factor in the impact of temperature on the death,  
104 metabolism, and reproduction rate of all lake species in  
105 the model, interpolating satellite data to describe water  
106 temperature and epilimnion depth. Our model is based  
107 on the principles of ecological stoichiometry, a robust  
108 modelling framework explicitly based on resource flows  
109 [31] that has been used to study algae-bacteria interac-  
110 tions and the impacts of toxin stress on trophic dynamics  
111 [30]. From empirical data, we simulate how tempera-  
112 ture and phosphorus variations will affect CBs and the  
113 health of fish populations in lakes with a wide variety of  
114 physical characteristics consistent with biological ranges.  
115 We showcase the practical applicability of our model by  
116 offering actionable management strategies for various  
117 north-temperate lakes. We fit our model to data from  
118 different lakes within Canada and the United States, al-  
119 lowing us to estimate key components of north-temperate  
120 lake ecosystems effectively.

## 121 Results

122 We simulated dynamics for several parameter configu-  
123 rations of lake conditions, including variations in water  
124 temperature, phosphorus input, water exchange, and epil-  
125 imnion depth. Specifically, we selected lakes with suffi-  
126 cient data from different mean phosphorus summertime  
127 (May 1 - Sep 30) concentrations. Referencing existing  
128 guidelines by the Canadian Council of Ministers of the  
129 Environment [32], we chose to simulate lakes with meso-  
130 eutrophic and hypereutrophic status. These configurations

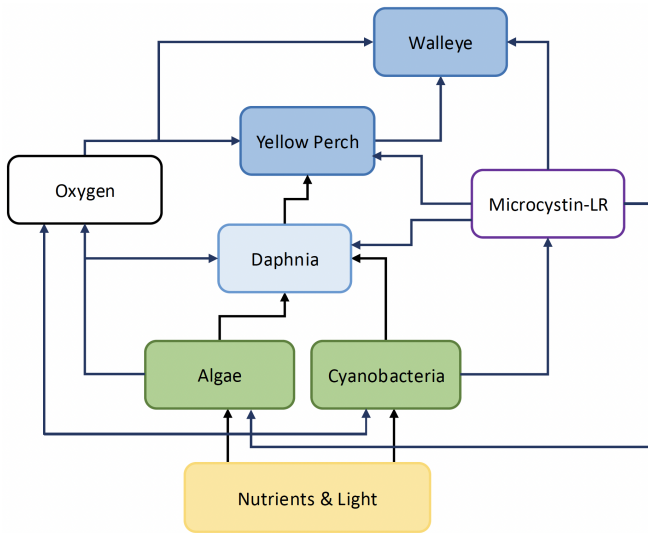


Figure 1: Schematic of production and consumption within the model. Based on the principles of ecological stoichiometry, we consider the input of nutrients and light on the growth of cyanobacteria and algae. We additionally introduce predator-prey dynamics of common freshwater species in north-temperate lakes: daphnia (which consume phytoplankton), yellow perch (which consume daphnia), and walleye (which eat the smaller yellow perch). This model structure also includes the bioaccumulation of toxins produced by cyanobacteria and absorbed into the various species. Finally, we assume oxygen is produced by cyanobacteria and algae through photosynthesis and consumed by daphnia and fish species and cyanobacterial biochemical oxygen demand.

species. Our simulations with increased lake temperature revealed a concerning and complex trend. They predict that height and duration of peak MC-LR concentrations vary depending on temperature. These values, reflecting a spectrum of potential scenarios influenced by population growth, economic development, and technological progress, emphasize the potential implications of future global temperature increases.

Yellow perch and walleye generally follow contrasting paths as the temperature rises. Walleye biomass decreases sooner in all four lakes as temperature increases, mainly owing to the heavy body burden – amount of toxin in an individual fish in units of mgMC-LR/mgC – of MC-LR carried by walleye due to either higher or earlier cyanobacterial activity (Figures 2, 3, S46, S52, and S61). Yellow perch biomass increases as temperature does in all lakes except Mendota (Figures 2 and 3). As walleye are a direct predator of yellow perch, they have a significant population resurgence near the summer’s end. However, the higher biomass of yellow perch is accompanied by a higher MC-LR body burden, although this is not nearly as severe as it is in walleye due to bioaccumulation.

Our simulation results indicate that initial phosphorus concentrations strongly influence cyanobacterial biomass and MC-LR concentrations. In all four lakes, increases in initial phosphorus dramatically increased cyanobacteria, algae and MC-LR and caused severe decreases in dissolved oxygen (Figures 4, S59, S45, and S51). This result delineates nutrient enrichment as a critical influence on CBs and their adverse environmental effects.

The influence variations on cyanobacterial biomass was also dependent on month. This is depicted in Figure 5, where we calculated the first- and total-order Sobol indices. These indices serve as statistical measures, assessing the sensitivity of model outputs to changes in input parameters and quantifying how variations in specific inputs influence model outcomes [33]. In May, the water exchange rate and turbidity were the dominant contributors to cyanobacterial biomass for all tested lakes. However, from June to early August, the influence variation of epilimnion depth steadily increased, while the variation of the other features decreased. Both the first- and total-order Sobol indices of epilimnion depth peaked in the middle of August. Towards the late warm season, the contributions of water exchange rate and phosphorus began to rise, with turbidity and lake temperature following suit after the warm season ended. The individual contribution of temperature is not as substantial as other individual factors, as shown by the first-order Sobol indices. However, temperature has a strong contribution to cyanobacterial biomass when

131 reflect a diverse array of lakes in North America, and we  
 132 identified critical influences on cyanobacteria concentra-  
 133 tion and MC-LR levels while considering the interactivity  
 134 of algae, daphnia, yellow perch, walleye, and dissolved  
 135 oxygen.

136 Specifically, we simulated various lake temperatures  
 137 by observing biologically reasonable ranges in north-  
 138 temperate dimictic lakes. Incrementally raising the wa-  
 139 ter temperature resulted in earlier and higher peaks for  
 140 cyanobacteria and MC-LR in lakes Mendota and Monona  
 141 in Wisconsin (Figures S46, S52). For Albertan lakes,  
 142 Pigeon lake and Pine lake, we observed the peaks of  
 143 MC-LR and cyanobacterial biomass occurring earlier.  
 144 However, the height of the peaks were only increased  
 145 for small to intermediate temperature increases (Figures  
 146 2, S61). These trends are mostly consistent for algal  
 147 biomass, except the peaks are higher than the baseline  
 148 for all increased temperatures. This subtle difference  
 149 is likely because they are the competing phytoplankton

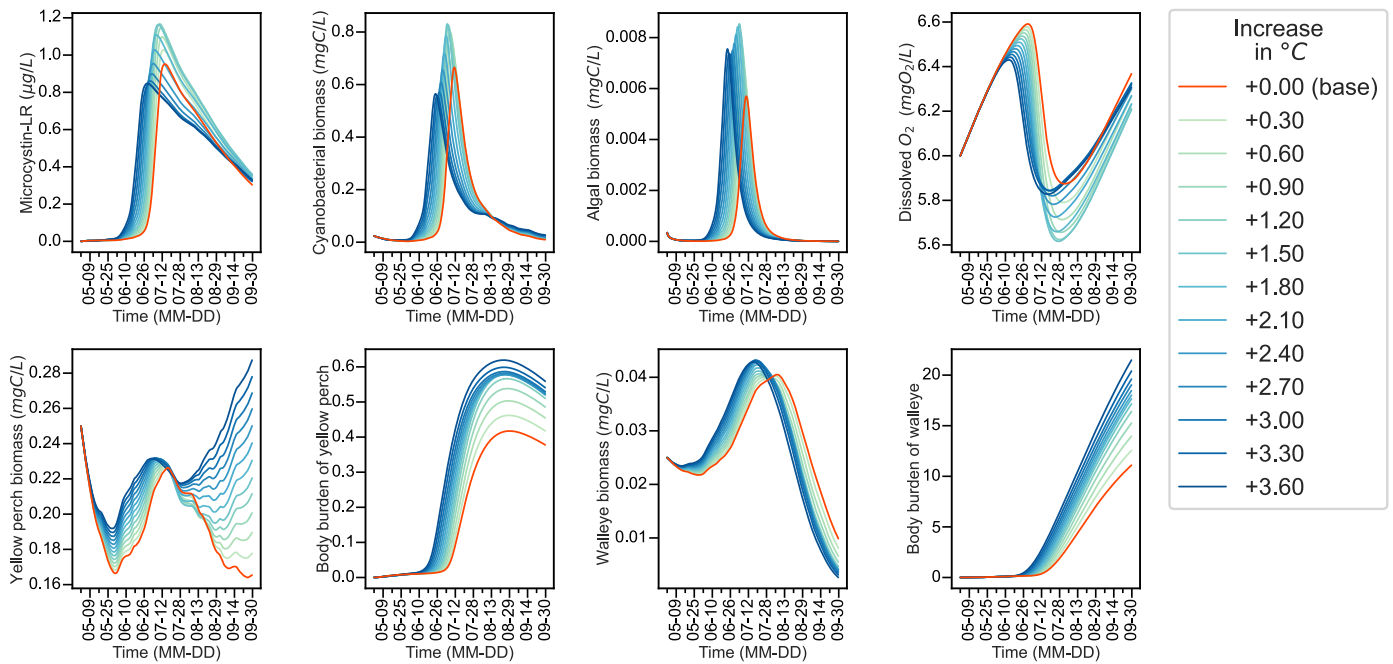


Figure 2: Impacts of temperature increases concentrated during the warm season (May to September 2021) on various ecosystem metrics in Pigeon Lake. The plots illustrate time series of MC-LR concentration, cyanobacterial biomass, algal biomass, dissolved oxygen concentration, yellow perch biomass, walleye biomass, and walleye and yellow perch body burden, for different temperature values compared to present conditions (+0.0°C, in red).

200 interacting with the other input parameters (Figures S63,  
 201 S62, and S64).

202 We used a vulnerability index – the MC-LR ratio  
 203 between outcomes for an increased temperature scenario  
 204 and the base scenario – to measure trends for lake charac-  
 205 teristics most at risk of CBs. We used three increased tem-  
 206 perature scenarios (+0.5°C, +1.5°C, and +3.5°C) based on  
 207 physically reasonable values [34] and the results are shown  
 208 in Figure 6. We found that lakes with low epilimnion  
 209 depth are the most vulnerable to heightened MC-LR con-  
 210 centrations once temperatures rise, consistent with their  
 211 greater propensity for CBs now [35]. The relationship  
 212 between the water exchange rate and MC-LR concen-  
 213 tration was more complex. The water exchange rate is  
 214 critical for shaping bloom characteristics. However, our  
 215 lower-medium warming scenarios for Pine Lake had aver-  
 216 age warm-season MC-LR concentrations rise at the same  
 217 relative proportions regardless of water exchange rate if  
 218 all else was equal. Further, low water exchange rates  
 219 exacerbate the increases in MC-LR seen in lakes with  
 220 shallow epilimnions under our severe warming scenar-  
 221 ios, indicating that the water exchange rate will rise in  
 222 importance as a factor as time goes on.

## Discussion

223  
 224 Primary exposure pathways for cyanotoxins such as MC-  
 225 LR include drinking water and recreational activities [36].  
 226 The consumption of fish from contaminated water is a  
 227 common but poorly studied route of human exposure [37].  
 228 We show that the body burden of MC-LR was more than  
 229 an order of magnitude higher in walleye than in yellow  
 230 perch; these results concur with prior field studies on toxin  
 231 bioaccumulation in freshwater fish [25, 30]. The severe  
 232 bioaccumulation observed poses critical threats to wildlife  
 233 conservation and public health. This indicates that fish  
 234 caught during and following CBs may pose significant  
 235 health risks and be unsafe for consumption [36, 38]. This  
 236 likewise represents a direct threat to human health through  
 237 consuming contaminated fish and terrestrial animals that  
 238 rely on these fish as a food source. Beyond immediate  
 239 toxicity, chronic exposure to cyanotoxins could lead to  
 240 long-term health effects, including liver damage [39],  
 241 cancer [40], and neurological disorders [41]. Humans  
 242 and other consumers of fish from lakes vulnerable to  
 243 CBs are at risk of secondary poisoning, which could lead  
 244 to population declines in already vulnerable species in  
 245 addition to the human health issues that arise. Given these  
 246 risks, comprehensive monitoring and regulation of fish

247 harvested from waters affected by CBs is urgently needed. 297  
248 Equally important is the need for public health advisories 298  
249 and guidelines on fish consumption during and after such 299  
250 events, as these measures are essential to protect both 300  
251 human and ecological health. 301

252 Our results delineate phosphorus and temperature as 302  
253 pivotal drivers in regulating the length and magnitude of 303  
254 CBs. The impact of temperature is particularly signifi- 304  
255 cant. Furthermore, we have shown that, in many cases, 305  
256 increases in temperature lead to notable increases in max- 306  
257 imum predicted MC-LR or earlier onset of peak MC-LR 307  
258 concentrations in the open water season (Figures 2, 3). 308  
259 Moreover, scenarios with larger temperature increases 309  
260 (+1.5°C and +3.5°C) raised MC-LR concentrations even 310  
261 higher (Figure 6). Similarly, increases in initial and input 311  
262 phosphorus concentrations lead to notably higher peak 312  
263 MC-LR concentrations (Figure 4). This emphasizes the 313  
264 need for nutrient management to mitigate bloom severity 314  
265 and toxicity, as controlling global temperatures is compar- 315  
266 atively futile. The growth of cyanobacteria significantly 316  
267 impacts the level of dissolved oxygen in lakes [42]. Our 317  
268 model shows that increased phosphorus concentrations 318  
269 can lead to significant oxygen depletion, causing strain 319  
270 on fish populations. This depletion is the most critical 320  
271 during the senescent phase of cyanobacteria, highlighting 321  
272 periods when lake oxygen, and thus aquatic life, are most 322  
273 vulnerable. 323

274 Several studies have explored the dynamics between 324  
275 environmental conditions and nutrient levels influencing 325  
276 CBs. We have observed similar trends that align with 326  
277 broader findings. For instance, Fernandez *et al.* [43] 327  
278 expect climate change to exacerbate conditions favourable 328  
279 to CBs in U.S. lakes, emphasizing the complex relation- 329  
280 ship between warmer water temperatures and increased 330  
281 nutrient runoff. Our results agree with this relationship, 331  
282 showing that a temperature increase of +3.5°C can cause 332  
283 earlier and higher peaks in MC-LR (Figures 2, S46, S52). 333  
284 Moreover, Wu *et al.* [44] found in their long-term study 334  
285 of Taihu Lake that increased phosphorus levels were sig- 335  
286 nificantly correlated with the frequency and intensity of 336  
287 CBs. Additionally, Heggerud *et al.* [10] found that phos- 337  
288 phorus concentrations were one of the critical values for 338  
289 predicting the onset of CBs. Our model produced similar 339  
290 results, where higher initial phosphorus concentrations 340  
291 led to substantial increases in MC-LR concentrations 341  
292 and peak cyanobacterial biomass. Although our results 342  
293 agree with a vast number of existing literature results, 343  
294 findings such as Hellweger *et al.* [45] suggest that the 344  
295 consideration of other macronutrients, such as nitrogen, is 345  
296 essential for accurately modelling cyanobacterial growth. 346

We assume that phosphorus is the limiting nutrient for 297  
our model, a biologically reasonable assumption based on 298  
the water quality of north-temperate dimictic lakes [46]. 299  
Therefore, we deem it sufficient to consider the dynamics 300  
of phosphorus as the overwhelming limiting nutrient for 301  
our model. However, the literature may benefit from 302  
models similar to ours considering nutrient co-limitation. 303

Our results indicate that shallower lakes experience 304  
drastic increases in cyanobacterial levels, leading to high 305  
MC-LR levels. In contrast, lakes with deeper epilimnion 306  
layers show significantly less severe blooms, suggesting 307  
that shallow lakes may need to be a priority for managers. 308  
Figure 6 shows shallow lakes are more vulnerable under 309  
increased temperature variations. Additionally, the wa- 310  
ter exchange rate affects bloom dynamics; a slow rate 311  
(0.02 m/day) maintains high toxin levels, whereas in- 312  
creasing the rate (0.12 m/day) drastically reduces MC-LR 313  
concentrations and mitigates oxygen depletion (Figure 314  
4). The relationship between water exchange rate and 315  
cyanobacteria has been studied previously. Zhang *et al.* 316  
[47] documented that an increase in the water exchange 317  
does not necessarily result in a decrease in cyanobac- 318  
teria concentration, nor MC-LR, due to the quality of 319  
the exchanged water. We observed a similar effect: the 320  
relationship between the water exchange rate and peak 321  
MC-LR can become non-monotonic under warmer lake 322  
temperatures. Our simulations also indicated that lakes 323  
with low epilimnion depth have both a greater propen- 324  
sity for CBs now and the most significant increase in 325  
cyanobacteria activity once temperatures rise (Figure 6). 326  
These results suggest that the lakes currently most sus- 327  
ceptible to CBs may become even more so, unfortunately 328  
experiencing no saturation effect relative to temperature 329  
in cyanobacterial activity. 330

The main factors that elicit substantial changes in 331  
CB characteristics were identified using Sobol indices 332  
and a series of simulations for each lake. These methods 333  
were carried out with different phosphorus concentrations, 334  
temperature changes, and physical lake characteristics 335  
(Figure 5). While epilimnion depth was observed to 336  
be a significant factor throughout the warm season, the 337  
water exchange rate, temperature increases, turbidity, 338  
and input phosphorus varied in both absolute and relative 339  
contributions to changes of CB characteristics as the warm 340  
season progressed. In particular, our findings suggest 341  
that rising temperatures, specifically in May and early 342  
June (i.e., earlier summers), can promote CBs in lakes 343  
regardless of their physical characteristics. However, the 344  
effects of heightened temperatures in September (i.e., 345  
longer summers) are more muted. Instead, phosphorus 346

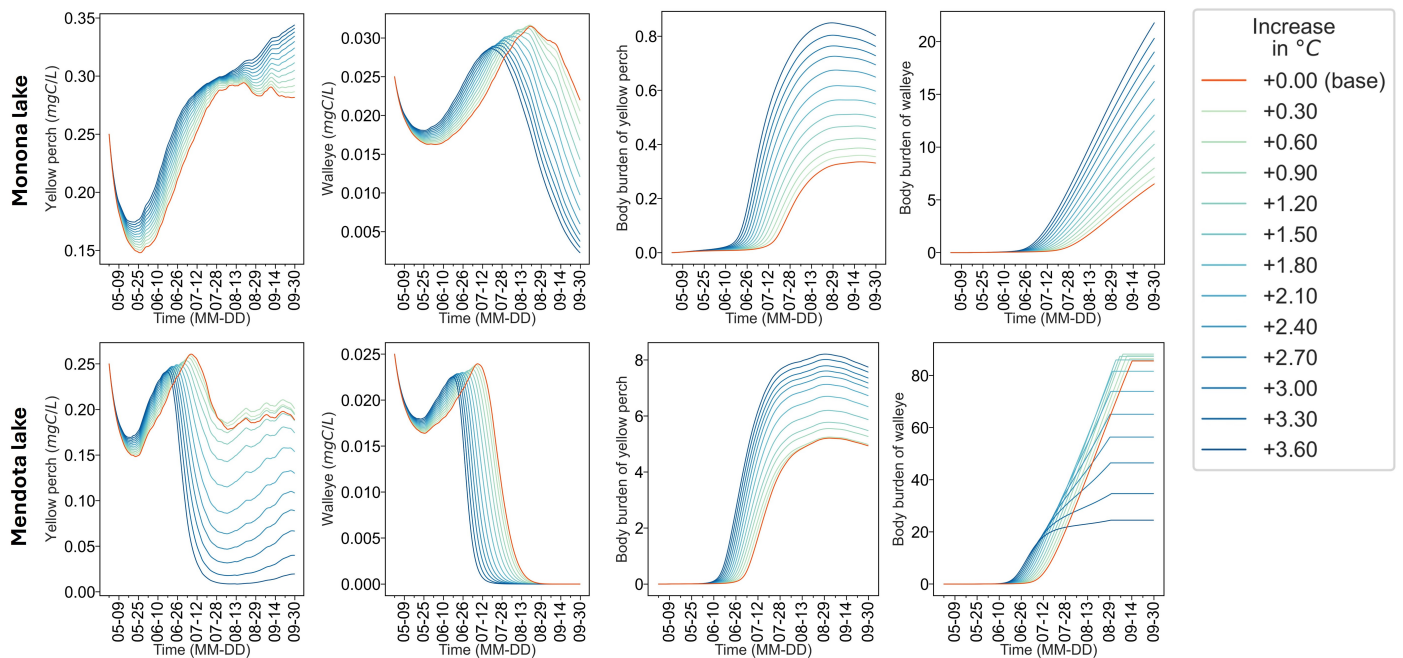


Figure 3: Impacts of temperature increases concentrated during the warm season on fish dynamics in Monona and Mendota Lakes. The plots illustrate time series of yellow perch and walleye biomass, and yellow perch and walleye body burden, for different temperature values compared to present conditions (+0.0°C, in red).

347 input plays a more significant role during the late warm  
 348 season, and more stagnant lakes with lower water exchange  
 349 rates are also more prone to cyanobacteria activity during  
 350 this time. These findings enable targeted interventions,  
 351 such as controlling phosphorus runoff in agricultural areas  
 352 or monitoring temperature changes in vulnerable lakes.

353 Future work should investigate the effects of other  
 354 limiting factors on phytoplanktonic growth. This would  
 355 include the availability of nitrogen, carbon, and micronu-  
 356 trients to provide a more comprehensive understanding  
 357 of nutrient interactions in bloom formation. Furthermore,  
 358 empirical evidence suggests that environments' spatial  
 359 scale and structure can influence population interactions  
 360 [48]. It would be informative (although complex) to  
 361 integrate within-lake spatial heterogeneity into our model,  
 362 following in the footsteps of prior modelling work focus-  
 363 ing on a single part of a lake ecosystem, e.g., [49, 50].  
 364 Remote sensing using satellite imagery could provide  
 365 accurate data to validate and refine such a spatial model  
 366 on the scale of a lake. Additionally, as climate change  
 367 continues to influence global water systems, longitudi-  
 368 nal modelling studies that track these changes will be  
 369 essential for developing better management strategies to  
 370 mitigate CBs' impact and downstream effects, such as the  
 371 bioaccumulation of toxins over a more extended period.

372 One limitation is the need for more data on oligo-  
 373 trophic lakes. Lakes classified as oligotrophic are

374 typically monitored less frequently due to the current  
 375 assumption that there is less propensity for CBs within  
 376 them, as they intuitively have lower levels of nutrients  
 377 for cyanobacteria to consume. While ample literature  
 378 supports this, emerging studies show the need to actively  
 379 monitor these lakes in an evolving world [51]. Lastly,  
 380 as this model is already very complex, an assumption  
 381 was made that walleye have no predators, only a natural  
 382 death rate exacerbated by hypoxic conditions. They also  
 383 do not expel the toxins back into the environment. This  
 384 leads the model to output low walleye populations during  
 385 the off-season due to their high body burden. While the  
 386 shallow values depicted by the model are an artifact of  
 387 its design, the broader qualitative dynamics that show  
 388 a summer peak followed by a decline in the fall are as  
 389 expected.

## 390 Materials and Methods

391 Our study aims to predict how drastically CBs would  
 392 be exacerbated by anthropogenic stressors (temperature  
 393 variation due to climate change and nutrient loading),  
 394 to ascertain the latent effects of these future blooms on  
 395 other lake organisms, and to determine how physical lake  
 396 characteristics can affect their resilience to heightened  
 397 cyanobacterial activity. To answer these questions, we de-

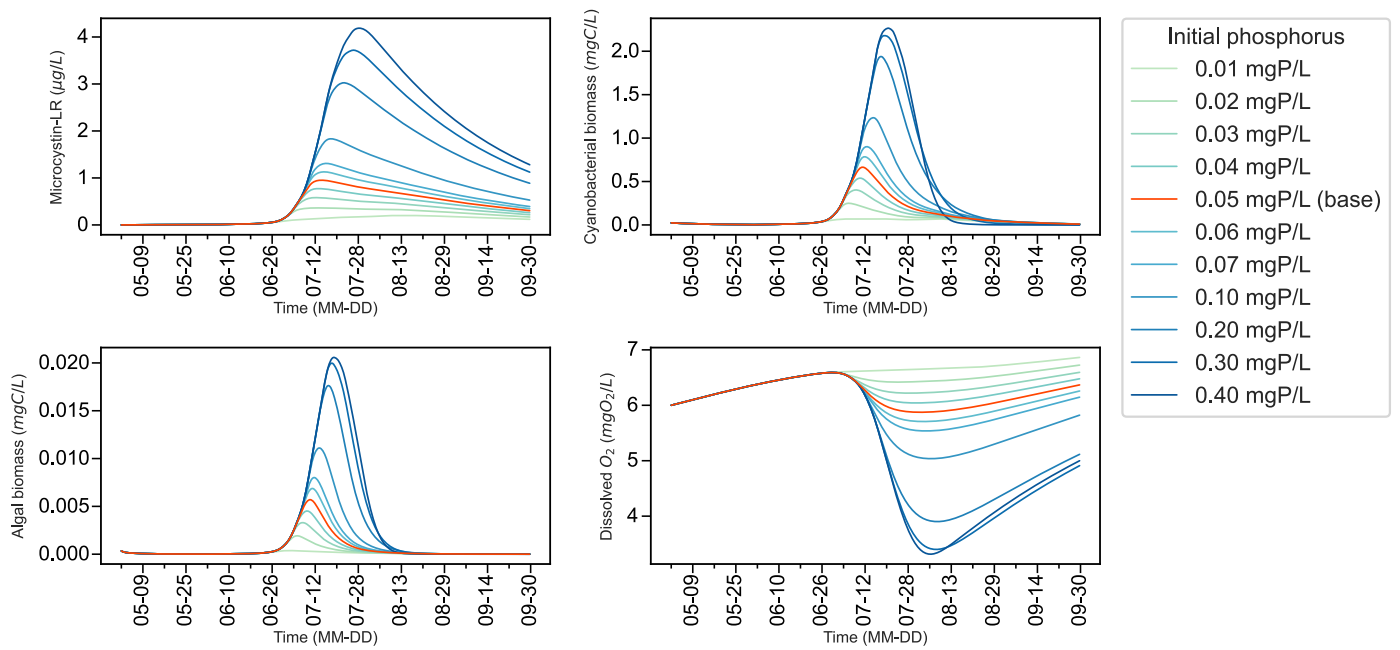


Figure 4: Impacts of initial phosphorus on various ecosystem metrics in Pigeon Lake. The plots illustrate time series of MC-LR concentration, cyanobacterial biomass, algal biomass, and dissolved oxygen concentration, for different initial phosphorus values compared to baseline conditions (0.05 mgP/L, in red).

398 developed a dynamical system model based on the principles  
 399 of ecological stoichiometry. The model represents a lake  
 400 food web with four trophic levels, incorporates the effects  
 401 of cyanobacteria on other lake organisms (secretion of  
 402 MC-LR and oxygen depletion) and explicitly features am-  
 403 bient water temperature, phosphorus concentration, and  
 404 other physical parameters relevant to cyanobacterial pop-  
 405 ulation dynamics (e.g. epilimnion depth, water exchange  
 406 rate). The Supplementary Information, SI 1, contains  
 407 comprehensive details on how the model was built.

## 408 Model formulation

409 We describe the dynamics of a freshwater ecosystem, in-  
 410 terconnecting several differential equations. For the lower  
 411 trophic levels in our model (cyanobacteria and algae), we  
 412 use an approach grounded in ecological stoichiometry,  
 413 focusing on macronutrients, energy, and temperature in-  
 414 teractions. Although including two phytoplankton species  
 415 (cyanobacteria and algae) adds complexity, it more accu-  
 416 rately depicts an aquatic environment, as not all unicellular  
 417 phytoplankton produce toxins and produces a more real-  
 418 istic diet for macro-invertebrates and herbivorous fish  
 419 species. Further complexification of the model through  
 420 more functional phytoplanktonic groups is deemed unnec-  
 421 essary for our purposes and unrealistic for data availability.  
 422 We use a Droop form for nutrient uptake and a Monod

form for light-dependent growth [52, 53], both empirically 423  
 supported [54], which capture the nuanced interactions 424  
 between abundances of cyanobacteria and algae, light 425  
 attenuation (modelled using the Lambert-Beer law [55, 426  
 56]), and nutrient availability. This approach is refined to 427  
 include specific adaptations of cyanobacteria, such as their 428  
 optimized growth in low-oxygen conditions, by adjusting 429  
 the standard growth equations to reflect these organisms' 430  
 distinct ecological roles and environmental responses [57]. 431  
 Droop kinetics for nutrient uptake and a Monod form for 432  
 light-dependent growth captures the inherent differences 433  
 in energy conversion. Light is quickly absorbed and 434  
 turned into usable energy, and the Monod form is ubiqui- 435  
 tous for the correlation between light and growth kinetics 436  
 [57–60]. Empirical evidence suggests that the Droop form 437  
 describes data more accurately for nutrient uptake despite 438  
 the increased mathematical complexity [54]. Tempera- 439  
 ture dependence is explicitly modelled using a cardinal 440  
 temperature model to describe the optimal growth tem- 441  
 peratures for algae and cyanobacteria. This assumption is 442  
 critical given the varying climatic conditions [14, 15, 61] 443  
 and their downstream effects on phytoplankton growth 444  
 rates [62]. In addition to cyanobacteria and algae, our 445  
 model features several common species that make up a 446  
 lake food web: daphnia, yellow perch, and walleye, which 447  
 are represented using consumer-resource dynamics. The 448  
 model also accounts for ecosystem feedback mechanisms, 449

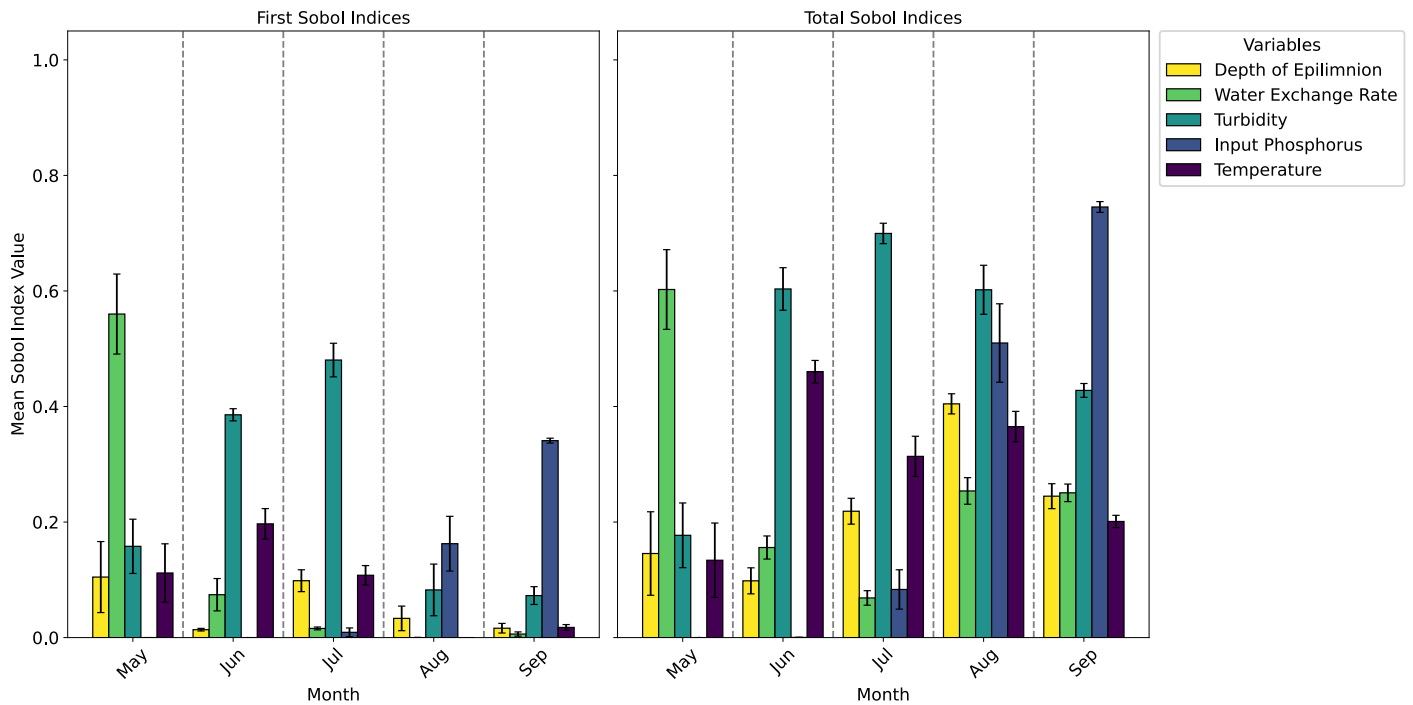


Figure 5: First-order (left) and total-order (right) Sobol indices for six model features: epilimnion depth, water exchange rate, turbidity, input phosphorus, and water temperature, in Pigeon lake, 2021. These indices vary each feature and calculate their direct (first-order) and combined direct and indirect (total-order) influence on cyanobacterial biomass.

450 which are essential for understanding the resilience of  
 451 aquatic species to CBs [63, 64]. A visual representation  
 452 of this model and its interactions is given in Figure 1.

### 453 Model fitting

454 Numerous datasets in our data availability section were  
 455 cleaned and appropriately combined for fitting. The stoi-  
 456 chiometric model was parameterized through a rigorous  
 457 process combining literature review and empirical data  
 458 from four lakes in North America. Based on their dis-  
 459 solved phosphorus levels and data availability, we selected  
 460 lakes for preliminary model fitting. Lake trophic classifi-  
 461 cations are by standards from the Canadian Water Quality  
 462 Guidelines for the Protection of Aquatic Life [32], which  
 463 define oligotrophic lakes as having total phosphorus con-  
 464 centrations less than 10  $\mu\text{g/L}$ , mesotrophic lakes between  
 465 10 and 35  $\mu\text{g/L}$ , and eutrophic lakes above 35  $\mu\text{g/L}$ . This  
 466 diverse selection of lakes allowed us to capture a broad  
 467 spectrum of ecological behaviours and interactions under  
 468 varying nutrient conditions, enhancing the robustness and  
 469 generalizability of our model across different lake types.

470 All parameters not found in the literature were esti-  
 471 mated by minimizing the mean square error between  
 472 observed and model-predicted data. See Table S.3 for all

detailed parameters and their appropriate citations. We  
 employed a differential evolution algorithm for parameter  
 optimization, allowing for a gradient-free search within  
 a hypercube of defined parameter constraints. Our algo-  
 rithm also used a fallback strategy to ensure meaningful  
 parameter outputs even in cases of numerical solver fail-  
 ure. The entire process was implemented in Python using  
 standard packages. Further details on the fitting process  
 and our algorithm are in the Supplementary Information;  
 SI 1.11.

### 483 Simulations

484 All simulations were performed using Python, with a  
 485 discretization step of 1/3 day. We used an independent  
 486 base case for each lake with parameters obtained from  
 487 model fitting. A time-dependent sensitivity analysis using  
 488 Sobol indices was conducted to evaluate the contribu-  
 489 tions of various physicochemical factors to cyanobacteria  
 490 biomass. The factors considered included epilimnion  
 491 depth, water exchange rate, turbidity, phosphorus input,  
 492 and water temperature. The vulnerability index was  
 493 calculated as the maximum MC-LR model output ratio  
 494 under increased water temperature, epilimnion depth, and  
 495 varying water exchange rates to the base case scenario



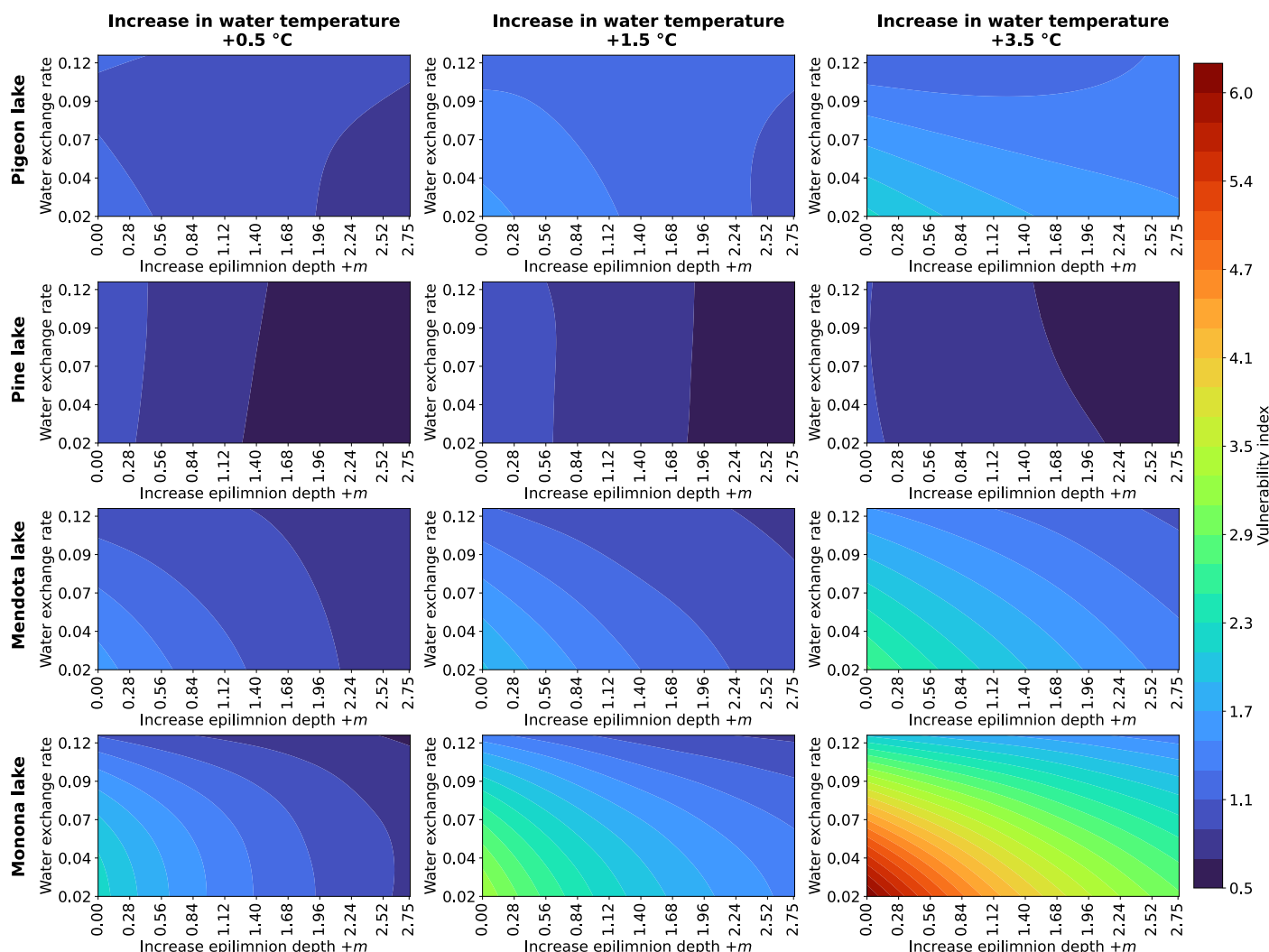


Figure 6: Vulnerability indices comparing the maximum MC-LR concentration under several warming scenarios to current values. This was done for varying water exchange rates (0.02 to 0.12 m/day) and increasing the epilimnion depth (+0 to +2.7 m) for four lakes. Each row represents Pigeon, Pine, Mendota, and Monona lakes. The columns represent increases in water temperature +0.5, +1.5, +3.5 °C, respectively, based on physically reasonable guideline values.

496 (without changes). Further details are provided in the  
 497 Supplementary Information.

## 498 Data Availability

499 The data that supports the findings of this study is available  
 500 on GitHub with the identifier Deciphering culprits CB.

## 501 Code Availability

502 The code that supports the findings of this study is avail-  
 503 able on GitHub with the identifier Deciphering culprits  
 504 CB.

## Acknowledgments

505 Our work was primarily supported by a grant from Alberta  
 506 Conservation Association. H.W. was partially supported  
 507 by an NSERC Individual Discovery Grant (RGPIN-2020-  
 508 03911), an NSERC Discovery Accelerator Supplement  
 509 Award (RGPAS-2020-00090), and a Tier 1 Canada Re-  
 510 search Chair. C.M.H. and A.H. were partially supported  
 511 by the US NSF grant no. 2025235. C.M.H. additionally  
 512 acknowledges the support of an NSERC PDF (PDF-  
 513 578392-2023). We would like to express our gratitude to  
 514 Peta Prokopiou for conducting a literature review during  
 515 the early stage. Grammarly was used to polish writing.  
 516

## References

- 517
- 518 [1] J. Huisman, G. A. Codd, H. W. Paerl, B. W. Ibelings, J. M. H. Verspagen, and P. M. Visser, Cyanobacterial blooms, *Nat. Rev. Microbiol.* **16**:pp. 471–483 2018
- 519
- 520
- 521 [2] Z. E. Taranu, R. W. Zurawell, F. Pick, and I. Gregory-Eaves, Predicting cyanobacterial dynamics in the face of global change: the importance of scale and environmental context, *Glob. Chang. Biol.* **18**:pp. 3477–3490 2012
- 522
- 523
- 524
- 525 [3] I. Chorus and M. Welker. *Toxic Cyanobacteria in water*. London: CRC Press, 2021.
- 526
- 527 [4] I. Stewart, A. A. Seawright, and G. R. Shaw, Cyanobacterial poisoning in livestock, wild mammals and birds—an overview, *Cyanobacterial harmful algal blooms: state of the science and research needs*:pp. 613–637 2008
- 528
- 529
- 530
- 531 [5] A. E. Poste, R. E. Hecky, and S. J. Guildford, Evaluating microcystin exposure risk through fish consumption, *Environ. Sci. Technol.* **45**:pp. 5806–5811 2011
- 532
- 533
- 534 [6] H. W. Paerl and T. G. Otten, Harmful cyanobacterial blooms: causes, consequences, and controls, *Microbial ecology* **65**:pp. 995–1010 2013
- 535
- 536
- 537 [7] H. W. Paerl, Mitigating harmful cyanobacterial blooms in a human- and climatically-impacted world, *Life (Basel)* **4**:pp. 988–1012 2014
- 538
- 539
- 540 [8] C. S. Zhao et al., Predicting cyanobacteria bloom occurrence in lakes and reservoirs before blooms occur, *Sci. Total Environ.* **670**:pp. 837–848 2019
- 541
- 542
- 543 [9] C. J. G. Loewen, F. R. Wyatt, C. A. Mortimer, R. D. Vinebrooke, and R. W. Zurawell, Multiscale drivers of phytoplankton communities in north-temperate lakes, *Ecol. Appl.* **30**:e02102 2020
- 544
- 545
- 546
- 547 [10] C. M. Heggerud et al., Predicting imminent cyanobacterial blooms in lakes using incomplete timely data, *Water Resources Research* **60**:e2023WR035540 2024
- 548
- 549
- 550 [11] L. M. V. Soares and M. do Carmo Calijuri, Deterministic modelling of freshwater lakes and reservoirs: Current trends and recent progress, *Environmental Modelling & Software* **144**:p. 105143 2021
- 551
- 552
- 553
- 554 [12] B. Bhagowati and K. U. Ahamad, A review on lake eutrophication dynamics and recent developments in lake modeling, *Ecohydrology & Hydrobiology* **19**:pp. 155–166 2019
- 555
- 556
- 557 [13] M. A. Frassl et al., A short review of contemporary developments in aquatic ecosystem modelling of lakes and reservoirs, *Environmental Modelling & Software* **117**:pp. 181–187 2019
- 558
- 559
- 560 [14] J.-P. Descy et al., Identifying the factors determining blooms of cyanobacteria in a set of shallow lakes, *Ecological Informatics* **34**:pp. 129–138 2016
- 561
- 562
- 563 [15] J.-F. Briand, C. Leboulanger, J.-F. Humbert, C. Bernard, and P. Dufour, *Cylindrospermopsis raciborskii* (cyanobacteria) invasion at mid-latitudes: Selection, wide physiological tolerance, or global warming? 1, *Journal of Phycology* **40**:pp. 231–238 2004
- 564
- 565
- 566
- 567
- 568 [16] A. Konopka and T. D. Brock, Effect of Temperature on Blue-Green Algae (Cyanobacteria) in Lake Mendota, *Applied and Environmental Microbiology* **36**:pp. 572–576 1978
- 569
- 570
- [17] H. Duan, C. Shang, K. Yang, and Y. Luo, Dynamic Response of Surface Water Temperature in Urban Lakes under Different Climate Scenarios—A Case Study in Dianchi Lake, China, *International Journal of Environmental Research and Public Health* **19**:p. 12142 2022
- [18] O. Desgué-Itier et al., Past and future climate change effects on the thermal regime and oxygen solubility of four peri-alpine lakes, *Hydrology and Earth System Sciences* **27**:pp. 837–859 2023
- [19] A. Giani, Z. E. Taranu, G. von Rückert, and I. Gregory-Eaves, Comparing key drivers of cyanobacteria biomass in temperate and tropical systems, *Harmful Algae* **97**:p. 101859 2020
- [20] S. B. Watson, E. McCauley, and J. A. Downing, Patterns in phytoplankton taxonomic composition across temperate lakes of differing nutrient status, *Limnol. Oceanogr.* **42**:pp. 487–495 1997
- [21] N. Bouaïcha et al., Structural diversity, characterization and toxicology of microcystins, *Toxins (Basel)* **11**:p. 714 2019
- [22] M. J. Brophy, B. F. Trueman, Y. Park, R. A. Betts, and G. A. Gagnon, Fluorescence spectra predict microcystin-LR and disinfection byproduct formation potential in lake water, *Environ. Sci. Technol.* **53**:pp. 586–594 2019
- [23] H. R. Shamsollahi, M. Alimohammadi, R. Nabizadeh, S. Nazmara, and A. H. Mahvi, Monitoring of microcystin-LR concentration in water reservoir, *dwt* **126**:pp. 345–349 2018
- [24] T. Guan et al., Open surface droplet microfluidic magnetosensor for microcystin-LR monitoring in reservoir, *Anal. Chem.* **92**:pp. 3409–3416 2020
- [25] B. G. Kotak, R. W. Zurawell, E. E. Prepas, and C. F. B. Holmes, Microcystin-LR concentration in aquatic food web compartments from lakes of varying trophic status, *Can. J. Fish. Aquat. Sci.* **53**:pp. 1974–1985 1996
- [26] S. Banerjee et al., Toxic effects of cyanotoxins in teleost fish: A comprehensive review, *Aquat. Toxicol.* **240**:p. 105971 2021
- [27] C. Malbrouck and P. Kestemont, Effects of microcystins on fish, *Environ. Toxicol. Chem.* **25**:pp. 72–86 2006
- [28] R. S. Shahmohammadloo, X. Ortiz Almirall, D. B. D. Simons, D. G. Poirier, S. P. Bhavsar, and P. K. Sibley, Fish tissue accumulation and proteomic response to microcystins is species-dependent, *Chemosphere* **287**:p. 132028 2022
- [29] L. Pearson, T. Mihali, M. Moffitt, R. Kellmann, and B. Neilan, On the chemistry, toxicology and genetics of the cyanobacterial toxins, microcystin, nodularin, saxitoxin and cylindrospermopsin, *Mar. Drugs* **8**:pp. 1650–1680 2010
- [30] F. J. Hardy, A. Johnson, K. Hamel, et al., Cyanotoxin bioaccumulation in freshwater fish, Washington State, USA, *Environmental Monitoring and Assessment* **187**:p. 667 2015
- [31] R. Sterner and J. J. Elser. *Ecological Stoichiometry: The Biology of Elements from Molecules to the Biosphere*. Princeton, NJ: Princeton University Press, 2002, p. 439.
- [32] C. C. of Ministers of the Environment. *Phosphorus: Canadian Water Quality Guidelines for the Protection of Aquatic Life*. Accessed: August 28, 2024. 2004.
- [33] I. M. Sobol, Global sensitivity indices for nonlinear mathematical models and their Monte Carlo estimates, *Mathematics and computers in simulation* **55**:pp. 271–280 2001

- 627 [34] ClimateData.ca. *Understanding Shared Socio-economic Path-*  
628 *ways (SSPs)*. [https://climatedata.ca/resource/](https://climatedata.ca/resource/understanding-shared-socio-economic-pathways-ssps/)  
629 [understanding-shared-socio-economic-pathways-](https://climatedata.ca/resource/understanding-shared-socio-economic-pathways-ssps/)  
630 [ssps/](https://climatedata.ca/resource/understanding-shared-socio-economic-pathways-ssps/). Accessed: 2023-10-18.
- 631 [35] H. W. Paerl and J. Huisman, Blooms like it hot, *Science*  
632 **320**:pp. 57–58 2008
- 633 [36] D. Stone and W. Bress, Addressing public health risks for  
634 cyanobacteria in recreational freshwaters: The Oregon and  
635 Vermont framework, *Integrated Environmental Assessment*  
636 *and Management* **3**:pp. 137–143 2009
- 637 [37] G. Codd, S. Bell, K. Kaya, C. Ward, K. Beattie, and J. Metcalf,  
638 Cyanobacterial toxins, exposure routes and human health,  
639 *European Journal of Phycology* **34**:pp. 405–415 1999
- 640 [38] W. Zhang et al., The Impact of Cyanobacteria Blooms on the  
641 Aquatic Environment and Human Health, *Toxins* **14**:p. 658  
642 2022
- 643 [39] T. Li et al., Advances in investigating microcystin-induced  
644 liver toxicity and underlying mechanisms, *Science of The*  
645 *Total Environment* **905**:p. 167167 2023
- 646 [40] S. Gu, M. Jiang, and B. Zhang, Microcystin-LR in Primary  
647 Liver Cancers: An Overview, *Toxins (Basel)* **14**:p. 715 2022
- 648 [41] J. S. Metcalf, M. Tischbein, P. A. Cox, and E. W. Stommel,  
649 Cyanotoxins and the Nervous System, *Toxins (Basel)* **13**:p. 660  
650 2021
- 651 [42] S. O’Boyle, G. McDermott, J. Silke, and C. Cusack, Potential  
652 impact of an exceptional bloom of *Karenia mikimotoi* on  
653 dissolved oxygen levels in waters off western Ireland, *Harmful*  
654 *Algae* **53**:pp. 77–85 2016
- 655 [43] M. Fernandez, T. E. Johnson, A. Shabani, and S. S. Lee,  
656 Geographic Analysis of the Vulnerability of U.S. Lakes to  
657 Cyanobacterial Blooms under Future Climate, *Earth Interac-*  
658 *tions* **27**: 2023
- 659 [44] S. Li, C. Liu, P. Sun, and T. Ni, Response of cyanobacterial  
660 bloom risk to nitrogen and phosphorus concentrations in  
661 large shallow lakes determined through geographical detector:  
662 A case study of Taihu Lake, China, *Science of The Total*  
663 *Environment* **816**:p. 151617 2022
- 664 [45] F. L. Hellweger et al., Models predict planned phosphorus  
665 load reduction will make Lake Erie more toxic, *Science*  
666 **376**:pp. 1001–1005 2022
- 667 [46] S. Bonilla et al., Nutrients and not temperature are the key  
668 drivers for cyanobacterial biomass in the Americas, *Harmful*  
669 *Algae* **121**:p. 102367 2023
- 670 [47] H. Zhang et al., Whether water exchange is an effective  
671 solution for emergency mitigation of algae bloom, *Journal of*  
672 *Water Process Engineering* **60**:p. 105085 2024
- 673 [48] R. S. Cantrell and C. Cosner. *Spatial Ecology via Reaction-*  
674 *Diffusion Equations*. John Wiley & Sons, Ltd, 2004.
- 675 [49] Y. Tao, S. A. Campbell, and F. J. Poulin, Dynamics of a  
676 diffusive nutrient-phytoplankton-zooplankton model with  
677 spatio-temporal delay, *SIAM Journal on Applied Mathematics*  
678 **81**:pp. 2405–2432 2021
- 679 [50] J. Zhang, J.-D. Kong, J. Shi, et al., Phytoplankton Competition  
680 for Nutrients and Light in a Stratified Lake: A Mathematical  
681 Model Connecting Epilimnion and Hypolimnion, *Journal of*  
682 *Nonlinear Science* **31**:pp. 1–35 2021
- [51] K. L. Reintjes et al., Cyanobacterial blooms in oligotrophic  
683 lakes: Shifting the high-nutrient paradigm, *Freshwater Biology*  
684 **66**:pp. 1846–1859 2021  
685
- [52] F. M. M. Morel, Kinetics of nutrient uptake and growth in  
686 phytoplankton, *Journal of Phycology* **23**:pp. 137–150 1987  
687
- [53] J. T. O. Kirk. *Light and Photosynthesis in Aquatic Ecosystems*.  
688 3rd ed. Cambridge University Press, 2010.  
689
- [54] H. Wang, P. V. Garcia, S. Ahmed, and C. M. Heggerud,  
690 Mathematical comparison and empirical review of the Monod  
691 and Droop forms for resource-based population dynamics,  
692 *Ecological Modelling* **466**:p. 109887 2022  
693
- [55] H. Wang, H. L. Smith, Y. Kuang, and J. J. Elser, Dynamics of  
694 Stoichiometric Bacteria-Algae Interactions in the Epilimnion,  
695 *SIAM Journal on Applied Mathematics* **68**:pp. 503–522 2007  
696
- [56] J. Huisman and F. J. Weissing, Light-Limited Growth and  
697 Competition for Light in Well-Mixed Aquatic Environments:  
698 An Elementary Model, *Ecology* **75**:pp. 507–520 1994  
699
- [57] C. M. Heggerud, H. Wang, and M. A. Lewis, Transient  
700 Dynamics of a Stoichiometric Cyanobacteria Model via  
701 Multiple-Scale Analysis, *SIAM Journal on Applied Math-*  
702 *ematics* **80**:pp. 1223–1246 2020  
703
- [58] E. M. Grima, F. G. Camacho, J. A. S. Pérez, J. M. F. Sevilla,  
704 F. G. A. Fernández, and A. C. Gómez, A Mathematical Model  
705 of Microalgal Growth in Light-Limited Chemostat Culture,  
706 *Journal of Chemical Technology & Biotechnology* **61**:pp. 167–  
707 173 1994  
708
- [59] S. Aiba. “Growth Kinetics of Photosynthetic Microorganisms”.  
709 *Microbial Reactions*. Ed. by A. Fiechter, S. Aiba, B. Atkinson,  
710 et al. Berlin, Heidelberg: Springer Berlin Heidelberg, 1982,  
711 pp. 85–156.  
712
- [60] P. H. C. Eilers and J. C. H. Peeters, Dynamic Behaviour of  
713 a Model for Photosynthesis and Photoinhibition, *Ecological*  
714 *Modelling* **69**:pp. 113–133 1993  
715
- [61] E. Van Derlinden and J. Van Impe, Modeling microbial  
716 kinetics as a function of temperature: identification of the  
717 growth/inactivation interface, *IFAC Proceedings Volumes*  
718 **43**:pp. 519–524 2010  
719
- [62] H. Cui, Y. Tao, J. Li, J. Zhang, H. Xiao, and R. Milne,  
720 Predicting and analyzing the algal population dynamics of a  
721 grass-type lake with explainable machine learning, *Journal*  
722 *of Environmental Management* **354**:p. 120394 2024  
723
- [63] A. Peace and H. Wang, Compensatory Foraging in Stochio-  
724 metric Producer–Grazer Models, *Bulletin of Mathematical*  
725 *Biology* **81**: 2019  
726
- [64] J. F. Haney, Field studies on zooplankton-cyanobacteria in-  
727 teractions, *New Zealand Journal of Marine and Freshwater*  
728 *Research* **21**:pp. 467–475 1987  
729

# Supplementary Information for “Deciphering culprits for cyanobacterial blooms and lake vulnerability in north-temperate lakes”

Jacob Serpico<sup>1,a</sup>, B. A. Zambrano-Luna<sup>1,a</sup>, Russell Milne<sup>1,a</sup>, Christopher M. Heggerud<sup>2</sup>, Alan Hastings<sup>2</sup>, and Hao Wang<sup>1,\*</sup>

<sup>1</sup>Interdisciplinary Lab for Mathematical Ecology and Epidemiology & Department of Mathematical and Statistical Sciences, University of Alberta, Edmonton, Alberta T6G 2R3, Canada

<sup>2</sup>Department of Environmental Science and Policy, University of California - Davis, California 95616, United States

<sup>a</sup>These authors contributed equally to this work.

\*Corresponding author: hao8@ualberta.ca

## 1 Model formulation

We explore the rigorous formulation of a dynamical system to model a north-temperate dimictic lake environment, which is one of the lake types where cyanobacterial blooms (CBs) can be particularly problematic, especially due to seasonal stratification and nutrient loading. Further, we explore the relevant biological mechanisms, assumptions, and constraints. There are 14 state variables in Table 1 for a complex, interconnected ordinary differential equation (ODE) model.

### 1.1 Stoichiometric dynamics of cyanobacteria and algae

We consider existing models from [1, 2] for the growth of phytoplankton in a freshwater aquatic ecosystem, with growth relying on macro-nutrients and light.

According to the Lambert-Beer law, the light intensity at the depth  $s$  of a water column with phytoplanktonic abundance  $U$  is given by

$$I(s, U) = I_{in} \exp[-(k_U U + K_{bg})s], \quad (1)$$

where  $I_{in}$ ,  $k_U$ , and  $K_{bg}$  are the light intensity at the water surface, species-specific light attenuation, and background light attenuation, respectively [3]. The light-dependent phytoplanktonic growth function employs the empirically supported and depth-dependent Monod form  $\frac{I(s,U)}{I(s,U)+H_U}$  [4] [5]. Here,  $H_U$  is the half-saturation constant of phytoplanktonic production. Assuming the epilimnion is well-mixed overnight due to the lake environment being dimictic [3] [5], we obtain the factor

$$h(U) \equiv \frac{1}{z_m} \int_0^{z_m} \frac{I(s, U)}{I(s, U) + H_U} ds = \frac{1}{z_m(k_U U + K_{bg})} \ln \left( \frac{H_U + I_{in}}{H_U + I(z_m, U)} \right) \quad (2)$$

for the depth-averaged phytoplanktonic growth function, where  $z_m$  is the mixing layer depth. Light is simultaneously absorbed and utilized by phytoplankton for energy; thus, the Monod form is ubiquitous for the correlation between light and growth kinetics [2, 6–8]. In contrast, nutrient uptake involves a two-step process (uptake and metabolism), enforcing the appropriateness of the Droop form for nutrient uptake [9]. Additionally, empirical evidence suggests that the Droop form describes data overwhelmingly more accurately for nutrient uptake despite the increased mathematical complexity [10]. The Droop term for phosphorus is given by  $1 - \frac{Q_{mU}}{Q_U}$ , where  $Q_{mU}$  is the minimum cell quota for phytoplankton, and  $Q_U$  is the associated variable cell quota. We obtain the phyto-

planktonic growth term by multiplying light and nutrient-dependent growth by the maximum reproduction rate,  $\mu_U$ . Due to the eventual complexity and primary purpose of the model, the complexification of the hydrodynamics through vertical spatial heterogeneity is unrealistic and unnecessary to incorporate.

We assume for variation that one of our functional groups for phytoplankton, algae, sink at the intersection of the epilimnion and hypolimnion, and its rate,  $\nu$ , is negatively related to the volume of epilimnion. Further, we assume that the algal sinking rate is inversely proportional to  $z_m$  [5]. We denote  $d_E$  as the combined water exchange rate between the epilimnion and hypolimnion and between the epilimnion and the external inflow and outflow. Similarly to [1], we assume that input phosphorus,  $p_{in}$ , is constant in the hypolimnion and the inflow.

Nutrient uptake is a decreasing function of phytoplanktonic cell quota. Uptake is maximal when the cell quota is  $Q_{mU}$  but should cease when the cell quota is  $Q_{MU}$ . Nutrient uptake follows the law of mass action [11], which is a saturating function of dissolved mineral phosphorous. These assumptions yield the nutrient uptake function

$$\rho(Q_U, P) = \rho_{mU} \left( \frac{Q_{MU} - Q_U}{Q_{MU} - Q_{mU}} \right) \frac{P}{M_U + P}, \quad (3)$$

where  $\rho_{mU}$  and  $M_U$  are the maximum phosphorus uptake rate and the half-saturation coefficient for phytoplanktonic phosphorus uptake, respectively. We apply this formulation to algae and cyanobacteria as our functional groups. Further, we consider cyanobacterial growth as a function of a variable cell quota. We do this since cyanobacteria have evolved optimized for conditions with little oxygen present and, therefore, rely on various other nutrients to increase their biomass. Furthermore, temperature and light conditions are pivotal when predicting cyanobacterial growth and blooms. This formulation is consistent with that of [2], and there is a visible similarity to the algal growth equation. Note that the objective is to model how CBs and resulting microcystin-LR (MC-LR) production affect higher trophic levels and, eventually, water quality; thus, two functional groups for phytoplankton are sufficient for this model and also reduce complexity due to the eventual solving of the model and data availability.

Accounting for both of our functional groups of phytoplankton, cyanobacteria ( $B$ ), and algae ( $A$ ), the light intensity factor for the depth-averaged growth functions are

$$h(A) \equiv \frac{1}{z_m(k_A A + k_B B + K_{bg})} \ln \left( \frac{H_A + I_{in}}{H_A + I(z_m, B, A)} \right), \quad (4)$$

and similarly

$$h(B) \equiv \frac{1}{z_m(k_A A + k_B B + K_{bg})} \ln \left( \frac{H_B + I_{in}}{H_B + I(z_m, B, A)} \right). \quad (5)$$

It is assumed that algae sink and cyanobacteria do not, and this is taken from plenty of literature, including [12]. We decided to include cell quota equations (P:C ratio) for both cyanobacteria and algae due to these species' more extensive homeostatic range.

## 1.2 Predator-prey dynamics

We assume that the predators have a Holling type II functional response and directly incorporate the carbon cost of feeding effort. We utilize ubiquitous empirically verified predator-prey equations [13]. Existing literature suggests

a suitable food web for our model: cyanobacteria and algae are our lowest trophic level of primary producers and have integral roles in aquatic ecosystems. Their primary consumption is by tiny crustaceans. We chose daphnia as the representative species as they are the keystone zooplankton in many dimictic lakes and reservoirs with existing literature modelling their dynamics [14] and data availability. Further, we let yellow perch be our consumer of daphnia since their diet consists primarily of zooplankton [15]. Lastly, we select the top trophic level, the piscivorous walleye, which frequently consumes yellow perch [16]. These functional groups adequately balance complexity with reality due to data availability in the chosen lake environments. Mathematically, these dynamics can be modelled with the following factors

$$f_B(B, A) = \frac{\phi\alpha_B B}{1 + \phi\alpha_B\tau_B B + \phi\alpha_A\tau_A A}, \quad (6)$$

$$f_A(B, A) = \frac{\phi\alpha_A A}{1 + \phi\alpha_B\tau_B B + \phi\alpha_A\tau_A A}, \quad (7)$$

representing the predation terms of cyanobacteria and algae, respectively,  $\phi$  is the water cleared/mgC invested to generate filtering energy, and  $\alpha_i$ ,  $\tau_i$  are the species-specific feeding cost and handling time, respectively. Since they are both consumed by daphnia, they are directly dependent on each other. Thus, they are both considered in the denominator. Similarly, the predation terms for daphnia  $D$  and yellow perch  $Y$  are given by

$$f_D(D) = \frac{\phi\alpha_D D}{1 + \phi\alpha_D\tau_D D}, \quad (8)$$

$$f_Y(Y) = \frac{\phi\alpha_Y Y}{1 + \phi\alpha_Y\tau_Y Y}. \quad (9)$$

In higher trophic levels like daphnia or fish, the complexity of nutrient dynamics increases significantly due to complex physiological regulation, trophic complexity, longer and multi-stage lives, and energy and nutrient allocation. Thus, we fix cell quotas for these species to avoid unnecessary complexity and uncertainty.

Further, for fish species  $i$  we propose a logistic growth limited by the carrying capacity  $\kappa_i$ , which is fitted and a portion of their diet given by a stable prey  $Ext_i$  [15].

### 1.3 MC-LR production

Using a similar formula for MC-LR production as [17], where an observed linear relationship between MC-LR production and cyanobacteria growth rate constructs the inferred equation

$$\frac{dM}{dt} = p\mu_B B \left(1 - \frac{Q_{mB}}{Q_B}\right) h(B) - d_M M, \quad (10)$$

where  $M$  is the MC-LR production in  $\mu\text{gC/L}$ ,  $p$  is the production coefficient of MC-LR, and  $d_M$  is the depletion rate.

## 1.4 Effect of MC-LR on various species

Due to the addition of toxins into the system, we need to consider the effect of MC-LR on various species. Observe that the toxin concentration within each species can be modelled similarly to the formulation by [13] to obtain

$$\left\{ \begin{array}{l}
 \frac{dV_A}{dt} = \underbrace{a_A MA}_{\text{uptake}} - \underbrace{\sigma_A V_A}_{\text{deporation due to metabolism}} - \underbrace{\mu_{r_A} V_A}_{\text{loss from respiration}} - \underbrace{\frac{v + d_E}{z_m} V_A}_{\text{loss from sinking and exchange}} - \underbrace{x_A v_A V_A}_{\text{loss from death}} - \underbrace{f_A(B, A) D v_A}_{\text{loss from predation}}, \\
 \frac{dV_D}{dt} = \underbrace{a_D MD}_{\text{uptake}} - \underbrace{\sigma_D V_D}_{\text{deporation due to metabolism}} - \underbrace{(x_D v_D + n_D) V_D}_{\text{loss due to death}} - \underbrace{f_D(D) Y v_D}_{\text{loss due to predation}} + \underbrace{f_B(B, A) D + f_A(B, A) D v_A}_{\text{gain due to predation}}, \\
 \frac{dV_Y}{dt} = \underbrace{a_Y MY}_{\text{uptake}} - \underbrace{\sigma_Y V_Y}_{\text{deporation due to metabolism}} - \underbrace{(x_Y v_Y + n_Y) V_Y}_{\text{loss due to death}} - \underbrace{f_Y(Y) W v_Y}_{\text{loss due to predation}} + \underbrace{f_D(D) Y v_D}_{\text{gain due to predation}}, \\
 \frac{dV_W}{dt} = \underbrace{a_W MW}_{\text{uptake}} - \underbrace{\sigma_W V_W}_{\text{deporation due to metabolism}} - \underbrace{(x_W v_W + n_W) V_W}_{\text{loss due to death}} + \underbrace{f_Y(Y) W v_Y}_{\text{gain due to predation}},
 \end{array} \right. \quad (11)$$

The general purpose of the terms is explained briefly underneath each one. The extensive list of parameters and state variables are described in Tables 1 and 3. To calculate the body burden  $v_i$ , we take the ratio  $V_i/i$  for each respective species  $i$  and compute the time derivative to obtain the body burden equations shown in equation (24). These equations describing species-specific toxin concentrations are coupled and complex, relying on each other and body burden.

## 1.5 Temperature dependence for cyanobacteria and algae dynamics

Understanding how temperature affects algae growth rates is essential for studying their behaviour in freshwater and brackish environments. Algae, along with cyanobacteria, play a vital role in aquatic ecosystems. With the increasing threat of nutrient pollution and global warming, the prevalence of cyanobacteria is predicted to rise as they thrive in high temperatures above 25°C. In comparison, algae grow optimally at approximately 27°C, [18–21]. To investigate these temperature dependencies, we will use a cardinal temperature model to study the optimal growth temperatures and the minimum and maximum temperature ranges that support their growth [22, 23]. Mathematically, we have

$$\eta_B(T) = \mu_B \left( \frac{(T - T_{min_B})^2 (T - T_{max_B})}{(T_{opt_B} - T_{min_B}) [(T_{opt_B} - T_{min_B})(T - T_{opt_B}) - (T_{opt_B} - T_{max_B})(T_{opt_B} + T_{min_B} - 2T)]} \right), \quad (12)$$

$$\eta_A(T) = \mu_A \left( \frac{(T - T_{min_A})^2 (T - T_{max_A})}{(T_{opt_A} - T_{min_A}) [(T_{opt_A} - T_{min_A})(T - T_{opt_A}) - (T_{opt_A} - T_{max_A})(T_{opt_A} + T_{min_A} - 2T)]} \right), \quad (13)$$

where  $T_{opt_B}$  is the optimal temperature for cyanobacterial growth.  $T_{min_B}$  and  $T_{max_B}$  are the lower and upper limits at which growth is 0 for cyanobacteria. In an analogous way,  $T_{opt_A}$  is the optimal temperature for algal growth.  $T_{min_A}$  and  $T_{max_A}$  are the lower and upper limits at which growth is 0 for algae.

## 1.6 The effect of temperature on daphnia and fish

The performance of consumers in an ecosystem is influenced by various factors such as temperature and nutrient availability. Among these factors, the thermal environment is a significant influencer for many organisms, [24,

25]. Aquatic vertebrates, invertebrates, and plants that are primarily ectothermic. The physiological processes of ectothermic organisms respond to changes in the thermal environment, as biological reactions are temperature-dependent. Consequently, these fluctuations lead to changes in assimilation and available energy, directly affecting an organism's growth, reproduction, overall fitness, and metabolic rate [26].

In a study conducted by Yurista *et al.* [25], it was observed that the assimilation efficiency (AE) of daphnia remains unaffected by changes in temperature. This finding led to the hypothesis that temperature does not significantly impact AE, which has been further explored in subsequent research, such as the study conducted by [24]. Further, in [26], the author conducted a study to investigate the relationship between temperature and the respiration rate of daphnia. They used a non-linear multivariate model, as proposed by Schoolfield [27], to analyze the data. The model's effectiveness was confirmed by validating it against experimental data. Following a similar process, we have

$$\delta_D(K) = \frac{\frac{K}{284} (0.01661) \exp(6866.7076(-0.05888 - 1/K))}{1 + \exp(-0.1148(-0.05888 - 1/K)) + \exp(-0.17172(-0.0913163 - 1/K))}, \quad (14)$$

where  $K = T + 273.15$  is the temperature in degrees Kelvin.

Cyclic and seasonal variations in fish's growth, reproduction, and physiological activities are intricately governed by the prevailing temperature and light (photoperiod) conditions in their environment. Among these factors, temperature is widely acknowledged as the foremost regulatory influence, as highlighted by [28]. Extensive research has demonstrated a positive correlation between temperature and both food conversion efficiency and methanolic rate, as reported in [29], [30], [28], and [31]. However, this positive relationship for food conversion efficiency holds only within specific temperature intervals, which vary significantly among different fish species. Once the temperature surpasses a certain threshold, typically the optimal temperature for a given fish species, this correlation transforms into a negative one [32, 33]. Utilizing data from [28] and [29], we derived a third-degree polynomial that aptly captures the general behaviour of conversion efficiency for walleye within the temperature range of 5 to 30 degrees Celsius, [34, 35]. Given the comparable behaviour exhibited by the yellow perch, as indicated in [28], we adopt a similar polynomial model for the yellow perch under analogous conditions. Thus, we will use the following function to improve conversion efficiency

$$E_{YW}(T) = e_{YW} \left( \frac{T^2(T - 30)}{24(24(T - 24) + 6(24 - 2T))} \right), \quad (15)$$

$$E_{YD}(T) = e_{YD} \left( \frac{T^2(T - 30)}{24(24(T - 24) + 6(24 - 2T))} \right). \quad (16)$$

Using the same idea, we fit a sigmoid function to understand the behaviour of the standard metabolic rate. The function is given by

$$\delta_W(T) = \delta_W (1 + \exp(-34.4467 * (T - 20.2893)))^{-0.00256}, \quad (17)$$

$$\delta_Y(T) = \delta_Y (1 + \exp(-34.4467 * (T - 20.2893)))^{-0.00256}. \quad (18)$$



## 1.7 Dissolved oxygen dynamics and the effect of oxygen depletion on mortality

Our study on dissolved oxygen dynamics involves a nonlinear mathematical model encompassing the processes leading to its depletion. The model postulates a constant growth rate of dissolved oxygen from various sources while its natural depletion rate is proportional to its concentration. Our research focuses on the contributions of algae and cyanobacteria, taking into account their respective growth rates. We also consider the depletion of dissolved oxygen resulting from the decomposition of cyanobacteria and the respiratory activities of yellow perch and walleye. Recognizing the aquatic ecosystem's complexity, we integrate daphnia's respiration into our model. This comprehensive approach enables us to understand the multifaceted interactions among different organisms and their impact on dissolved oxygen levels in aquatic environments, [36–38]. The oxygen equation is explicitly given by

$$\frac{dO}{dt} = \underbrace{q_{air}}_{\text{exchange of oxygen with air}} - \underbrace{q_d O}_{\text{depletion to the air}} + \underbrace{\delta_A A \left(1 - \frac{Q_{m_A}}{Q_A}\right) h(A) \eta_A(T)}_{\text{oxygen produced by algae}} \quad (19)$$

$$+ \underbrace{\delta_B^+ B \left(1 - \frac{Q_{m_B}}{Q_B}\right) h(B) \eta_B(T)}_{\text{oxygen produced by cyanobacteria}} - \underbrace{\delta_B^- N_B(T) B - \delta_D D - \delta_Y Y - \delta_W W}_{\text{oxygen used}}. \quad (20)$$

Water bodies' dissolved oxygen levels are crucial for fish survival as they impact their growth, development, and physiological processes. CBs are a primary concern as they reduce dissolved oxygen levels. In severe cases, the oxygen deficit can lead to massive fish mortality, resulting in significant economic losses for the aquaculture industry, [39–42].

To better understand this phenomenon, we have employed a sigmoid function to model the relationship between mortality and dissolved oxygen. This model considers the critical threshold for hypoxia and the recommended minimum dissolved oxygen levels necessary for fish. It provides quantitative insight into fish mortality's complex dynamics in response to dissolved oxygen levels, [40, 41]. These equations are depicted as

$$N_Y(O) = \frac{1}{1 + e^{3.1209(O-4.01131)}}, \quad (21)$$

$$N_W(O) = \frac{1}{1 + e^{3.516129(O-4.09359)}}, \quad (22)$$

where  $O$  is the dissolved oxygen and  $O_{min_Y}$ ,  $O_{min_W}$  are asphyxiation points and  $O_{nor} = 6\text{mg}/L$  is the minimal dissolved oxygen for healthy fish populations. Both curves were fitting such that  $N_Y(O_{nor}) \approx n_Y$  and  $N_W(O_{nor}) \approx n_W$  for  $O \geq O_{nor}$ , and  $N_Y(O) = N_W(O) = 1$  for  $O < O_{min_Y}$  and  $O < O_{min_W}$ , respectively.

## 1.8 Cellular MC-LR content

Following the findings in [43], there is a definite linear correlation between the amount of cellular MC-LR content (MC-LR quotas) and the reproduction rate of cyanobacteria. This finding is consistent with the results of other experiments, as documented in [44]. In this paper, we use a similar framework, taking into account the fluctuations of cyanobacteria reproduction rate in response to changes in temperature. To ensure consistency, we convert the

formulation from [43], which was initially expressed in mol/cell, to alternative units of  $\mu\text{g}/\text{cell}$  (taking into account the molar mass of 1008 g/mol, as referenced in [45]) and to  $\mu\text{g}/\text{mgC}$ . We convert cyanobacteria counts (cell) to carbon (mg C) using the factor ( $14.12376 \times 10^{-9} \text{mgC}/\text{cell}$ ) or ( $1.176 \text{pmol C}/\text{cell}$ ), taking the average of the carbon concentration per cell obtained in [46]. This unit conversion ensures accuracy and coherence in our analysis. The equation is given by

$$Q_{\text{MCYST}}(T) = 4.703283\eta_B(T) \left(1 - \frac{Q_{m_B}}{Q_B}\right) h(B) + 3.5685. \quad (23)$$

## 1.9 Lake temperature and epilimnion depth as a function of time

We calculated the temporal temperature and epilimnion depth profile of the lake,  $T(t)$ ,  $Z_m(t)$ , by applying the Akima interpolation method using the dataset from Era5-Land; it is a reanalysis dataset providing a consistent view of the evolution of land variables over several decades at an enhanced resolution, [47]. Akima method uses third-degree polynomials to interpolate between data points, offering enhanced accuracy, [48, 49]. We obtained the water temperature and epilimnion depth using Google Earth Engine, [50] taking the average over the lakes each day of the warm season. We used the lake shape provided by datasets as the areas of interest, [51–53].

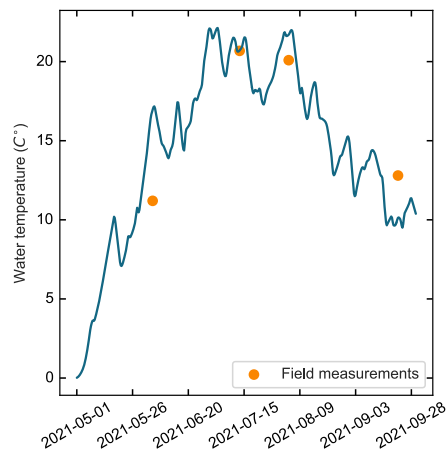


Figure 1: Example water temperature at the thickness of the uppermost layer of an inland water body (blue line). Additional in-site measurements are provided by the orange points.

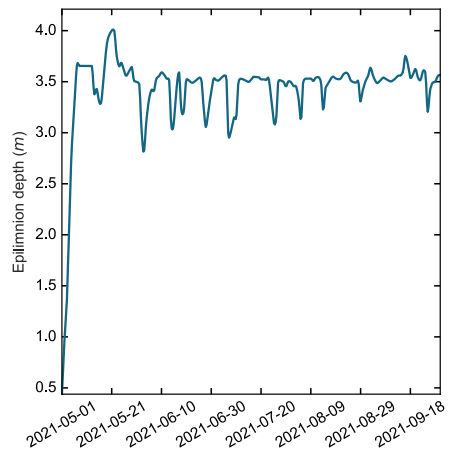


Figure 2: Example of epilimnion depth for the thickness of the uppermost layer of an inland water body (blue line).

## 1.10 Full model

The complete model, containing all of the state variables and processes discussed above, is as follows:

$$\begin{aligned}
\frac{dM}{dt} &= \underbrace{p\eta_B(T)B \left(1 - \frac{Q_{mB}}{Q_B}\right) h(B)}_{\text{MC-LR production}} - \underbrace{d_M M}_{\text{depletion}} \\
\frac{dB}{dt} &= \underbrace{\eta_B(T)B \left(1 - \frac{Q_{mB}}{Q_B}\right) h(B)}_{\text{limited growth}} - \underbrace{\mu_{rB} B}_{\text{respiration}} - \underbrace{\frac{d_E}{z_m} B}_{\text{exchange}} - \underbrace{f_B(B, A)D}_{\text{predation}}, \\
\frac{dA}{dt} &= \underbrace{\eta_A(T)A \left(1 - \frac{Q_{mA}}{Q_A}\right) h(A)}_{\text{limited growth}} - \underbrace{\mu_{rA} A}_{\text{respiration}} - \underbrace{\frac{v + d_E}{z_m} A}_{\text{sinking and exchange}} - \underbrace{x_A v_A A}_{\text{toxin death}} - \underbrace{f_A(B, A)D}_{\text{predation}}, \\
\frac{dD}{dt} &= \underbrace{e_{BD} \min\left\{1, \frac{Q_B}{\theta_D}\right\} f_B(B, A)D + e_{AD} \min\left\{1, \frac{Q_A}{\theta_D}\right\} f_A(B, A)D}_{\text{gain from growth}} - \underbrace{(\alpha_A + \alpha_B)D}_{\text{cost of feeding}} - \underbrace{(x_D v_D + n_D)D}_{\text{death}} - \underbrace{j_Y f_D(D)Y}_{\text{predation}}, \\
\frac{dY}{dt} &= \underbrace{r_Y E_{DY}(T) (j_Y f_D(D) + (1 - j_Y) \text{Ext}_Y) Y (1 - Y/\kappa_Y)}_{\text{gain from growth}} - \underbrace{\alpha_D Y}_{\text{cost of feeding}} - \underbrace{(x_Y v_Y + N_Y(O))Y}_{\text{death}} - \underbrace{j_W f_Y(Y)W}_{\text{predation}}, \\
\frac{dW}{dt} &= \underbrace{r_W E_{YW}(T) (j_W f_Y(Y) + (1 - j_W) \text{Ext}_W) W (1 - W/\kappa_W)}_{\text{gain from growth}} - \underbrace{\alpha_Y W}_{\text{cost of feeding}} - \underbrace{(x_W v_W + N_W(O))W}_{\text{death}}, \\
\frac{dQ_B}{dt} &= \underbrace{\rho(Q_B, P)}_{\text{replenishment}} - \underbrace{Q_B \mu_B \left(1 - \frac{Q_{mB}}{Q_B}\right) h(B)}_{\text{loss due to cyanobacteria growth}}, \\
\frac{dQ_A}{dt} &= \underbrace{\rho(Q_A, P)}_{\text{replenishment}} - \underbrace{Q_A \mu_A \left(1 - \frac{Q_{mA}}{Q_A}\right) h(A)}_{\text{loss due to algal growth}}, \\
\frac{dP}{dt} &= \underbrace{\frac{d_E}{z_m} (p_{in} - P)}_{\text{P input and exchange}} - \underbrace{\rho(Q_A, P)A}_{\text{consumption by algae}} - \underbrace{\rho(Q_B, P)B}_{\text{consumption by cyanobacteria}}, \\
\frac{dv_A}{dt} &= \underbrace{a_A M}_{\text{uptake}} - \underbrace{\sigma_{AV} v_A}_{\text{deperation due to metabolism}} - \underbrace{\mu_A \left(1 - \frac{Q_{mA}}{Q_A}\right) h(A) v_A}_{\text{dilution due to birth and growth}}, \\
\frac{dv_D}{dt} &= \underbrace{a_D M}_{\text{uptake}} - \underbrace{\sigma_{DV} v_D}_{\text{deperation due to metabolism}} + \underbrace{f_B(B, A)Q_{MCYST}(T) + f_A(B, A)v_A}_{\text{gain due to predation}} \\
&\quad - \underbrace{e_{BD} \min\left\{1, \frac{Q_B}{\theta_D}\right\} f_B(B, A)v_D - e_{AD} \min\left\{1, \frac{Q_A}{\theta_D}\right\} f_A(B, A)v_D}_{\text{dilution due to birth and growth}}, \\
\frac{dv_Y}{dt} &= \underbrace{a_Y M}_{\text{uptake}} - \underbrace{\sigma_{YV} v_Y}_{\text{deperation due to metabolism}} + \underbrace{f_D(D)v_D}_{\text{gain due to predation}} - \underbrace{E_{DY}(T)f_D(D)v_Y}_{\text{dilution due birth and growth}}, \\
\frac{dv_W}{dt} &= \underbrace{a_W M}_{\text{uptake}} - \underbrace{\sigma_{WV} v_W}_{\text{deperation due to metabolism}} + \underbrace{f_Y(Y)v_Y}_{\text{gain due to predation}} - \underbrace{E_{YW}(T)f_Y(Y)v_W}_{\text{dilution due to birth and growth}}, \\
\frac{dO}{dt} &= \underbrace{q_{air}}_{\text{exchange of oxygen with air}} - \underbrace{q_{dO}}_{\text{depletion to the air}} + \underbrace{\delta_{AA} \left(1 - \frac{Q_{mA}}{Q_A}\right) h(A)\eta_A(T)}_{\text{oxygen produced by algae}} + \underbrace{\delta_B^+ B \left(1 - \frac{Q_{mB}}{Q_B}\right) h(B)\eta_B(T)}_{\text{oxygen produced by cyanobacteria}} \\
&\quad - \underbrace{\delta_B^- N_B(T)B - \delta_D(T)D - \delta_Y(T)Y - \delta_W(T)W}_{\text{oxygen used}}. \tag{24}
\end{aligned}$$

## 1.11 Model fitting

As with all models, the accurate and consistent configuration of parameters is crucial for aligning the model with real-world experiments. Stoichiometric models typically necessitate experimental and laboratory measurements to tailor a model to specific situations. We conducted an extensive literature review to identify appropriate values that would allow us to ground our model in concrete conditions, enhancing its real-world accuracy. Despite not finding all the parameters required by our model, we leveraged comprehensive data spanning lakes and years [54] including Canada and US government open information. These extensive datasets facilitated the development of a more generalized and applicable model, and we used this dataset to estimate those parameters that were previously unavailable to us.

We estimated the parameters by minimizing the mean square error between the data points in our dataset that describe the cyanobacteria, dissolved oxygen, and MC-LR concentration and the solution of our model. We first transformed the cyanobacteria concentration units of the dataset from cells/L to C mg/L, which represents carbon biomass, using the conversion factor of  $14.12376 \times 10^{-9}$  C mg/cell [46]. Following this transformation, we minimized the mean square error defined by

$$J_X = \frac{1}{n} \sum_{i=1}^n (y_{d_i} - X(d_i))^2,$$

where  $X$  is cyanobacteria, dissolved oxygen or MC-LR concentration,  $n$  is the number of measurements we have for a specific lake during May 1-September 30 of a given year and specific variable, and  $d_i$  is the day that the sample was taken. We minimized the average mean square error for each variable,  $J = 1/3(J_B + J_M + J_O)$ .

Given the considerable size of our model, we opted for a different approach to minimize  $J$  that does not rely on the function's gradient. Instead, we employed a "differential evolution" algorithm, a stochastic, population-based optimization technique already implemented in Python [55], the differential evolution method. This algorithm enables us to find a local minimum through an extended and initial random search without any assumptions about the gradient of our model. We also imposed constraints on the parameters, restricting them to be greater than zero, which is the weakest assumption one can impose on parameters with biological meaning. In addition to these constraints, we defined a hypercube within which the algorithm must find the configuration of parameters that minimize our function. This hypercube was determined by a greedy algorithm assuming that the species should survive throughout the year without MC-LR and that the parameters should be greater than zero. In other words, we restricted that the minimum values of all variables, other than body burden and MC-LR, should be greater than  $10^{-3}$  (see Table 2 for the hypercube). Finally, in cases where the numerical solver was unsuccessful under some combination of parameters, we defined  $B(d_i) = -1$ ,  $M(d_i) = -1$ , or  $O(d_i) = -1$  for all days  $d_i$ . This process ensures that the configuration of parameters we find is also suitable for obtaining a numerical solution to our model, thereby enhancing the accuracy of the chosen parameters in a real scenario. The entire implementation was done in Python using standard packages such as Pandas, Numpy, and Scipy. The initial conditions for all simulations can be found in our available code section 1.13.

## 1.12 Sobol Indices

We investigated how various external factors affect the overall configuration of lakes throughout the year. These factors include different water exchange rates ( $d_E$ ), turbidity ( $K_{bg}$ ), phosphorus input ( $p_{in}$ ), and the increase of depth of the epilimnion ( $z_m$ ) and water temperature. To evaluate the impact of each parameter, we employed the method proposed by Sobol [56]. This method uses Monte Carlo to calculate complex models' global sensitivity indices. We calculate the first-order and total-order Sobol indices. The first-order index independently identifies each factor's contribution to the cyanobacteria prediction; meanwhile, the total-order index identifies each factor's contribution, including its direct influence and interactions with other factors. The first-order index is calculated for each factor  $f$  as

$$SI_f(t) = \frac{\text{Var}[\mathbb{E}[B(t)|X_f]]}{\text{Var}[B(t)]}$$

and the total-order index as

$$ST_f = 1 - \frac{\text{Var}[\mathbb{E}_{\sim f}[B(t)|f]]}{\text{Var}[B(t)]},$$

where  $\mathbb{E}_{\sim f}[B(t)|f]$  is the expectation of  $B(t)$  with respect to all factors except  $f$ . We estimated the first-order and total-order indices using the Python package SALib [57]. We generated 14336 random configurations under the condition that increase of depth of the epilimnion is in  $[0, 2.75]$ ,  $d_E$  is in  $[0.02, 0.12]$ ,  $K_{bg}$  is in  $[0.3, 1.0]$ ,  $p_{in}$  is in  $[0.01, 0.4]$ , and water temperature increase is in  $[0, 3.4]$ .

### 1.13 Simulations

All the numerical analyses were performed using Python. All the codes and datasets are available on Deciphering culprits CB:

First, we created a daily dataset for each lake and corresponding year with the average water temperature and depth of the epilimnion across the lake using the shoreline Boundary (GIS data) we collected, section 1.9 (WaterTemperature.py script). Then, we implemented the model with all the parameters presented in Table S.3, making the unknown parameters as empty values (model\_v1\_8.py script). For each lake, we determined its corresponding unknown parameters, which were found using the in-site measurements, section 1.11. Third, each simulation was run independently for each lake (plot\_full\_model\_params\_v1\_8\_year.py and plot\_full\_model\_params\_fitted.py); this includes the vulnerability index (Vulnerability indices.ipynb) and Sobol indices (First-order and total Sobol index.ipynb). All the parameters found after fitting, which were used during the research, are available in "FittedParameters" folder with their respective lake names. All the data generated to create the vulnerability indices and Sobol indices are also available and can be plotted using "First-order and total Sobol index\_plotting.ipynb" and "Plotting heatmaps vulnerability.ipynb". The table with all our model's parameters is in the folder "ParametersODE".

## 2 Figures and Tables

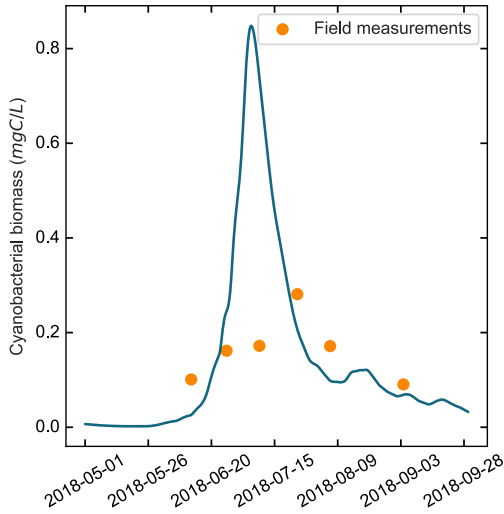


Figure 3: Predicted cyanobacterial biomass after fitting dynamical system model to data from Mendota lake, Wisconsin, United States, 2018.

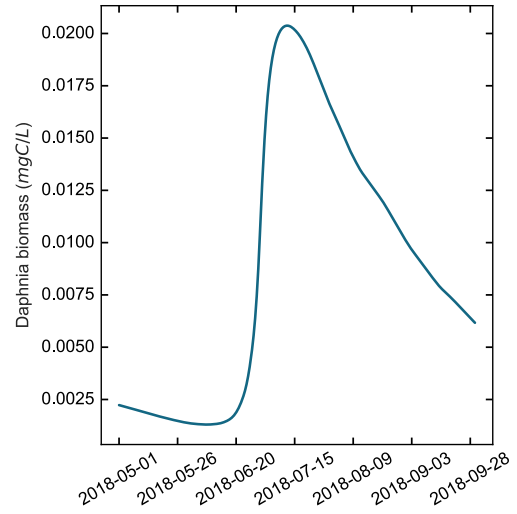


Figure 5: Predicted daphnia biomass after fitting dynamical system model to data from Mendota lake, Wisconsin, United States, 2018.

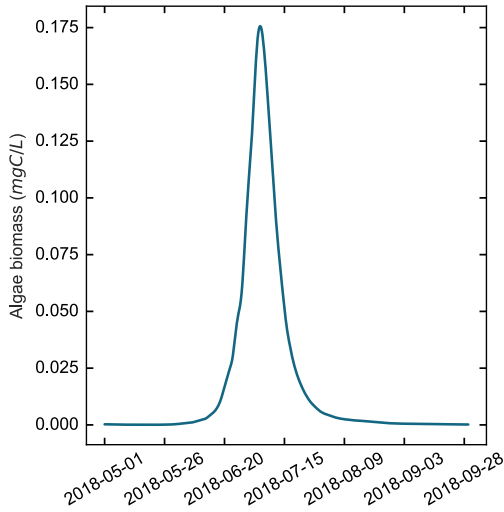


Figure 4: Predicted algal biomass after fitting dynamical system model to data from Mendota lake, Wisconsin, United States, 2018.

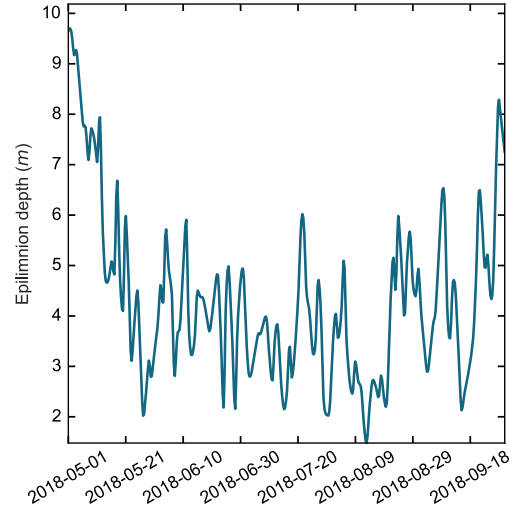


Figure 6: Satellite data for epilimnion depth from Mendota lake, Wisconsin, United States, 2018.



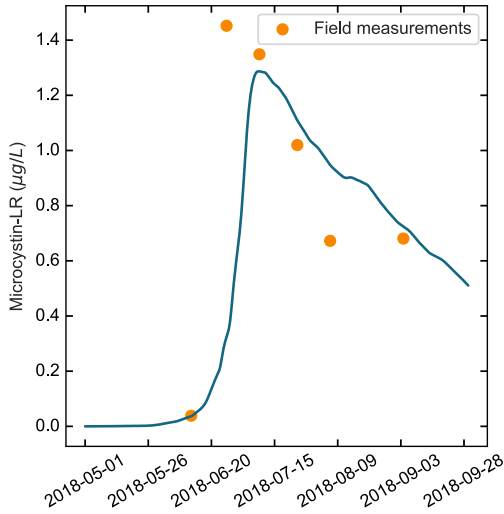


Figure 7: Predicted MC-LR concentration after fitting dynamical system model to data from Mendota lake, Wisconsin, United States, 2018.

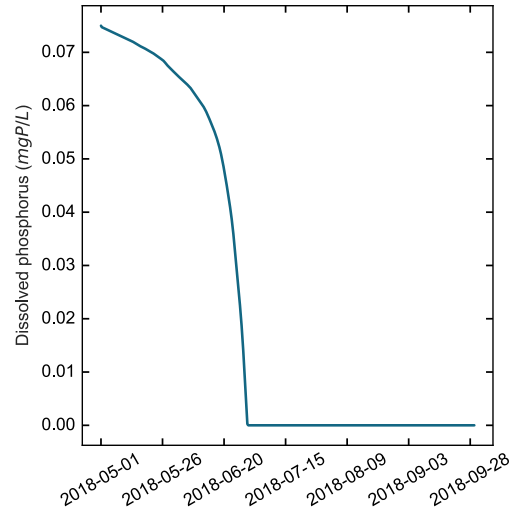


Figure 9: Annual prediction for cyanobacteria after fitting dynamical system model to data from Mendota lake, Wisconsin, United States, 2018.

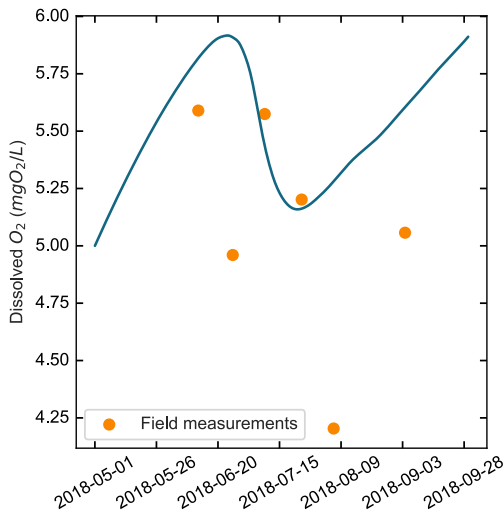


Figure 8: Satellite data for dissolved lake oxygen from Mendota lake, Wisconsin, United States, 2018.

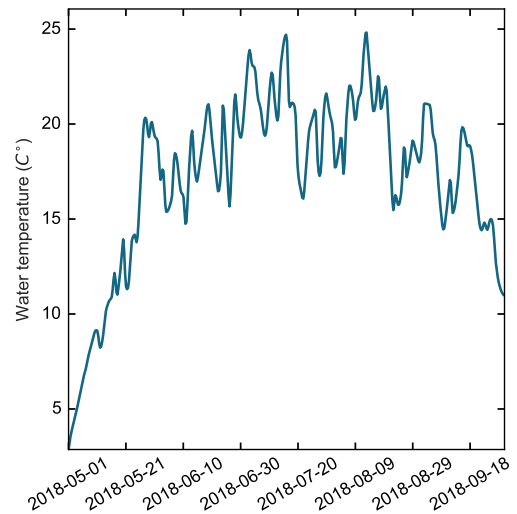


Figure 10: Satellite data for water temperature from Mendota lake, Wisconsin, United States, 2018.

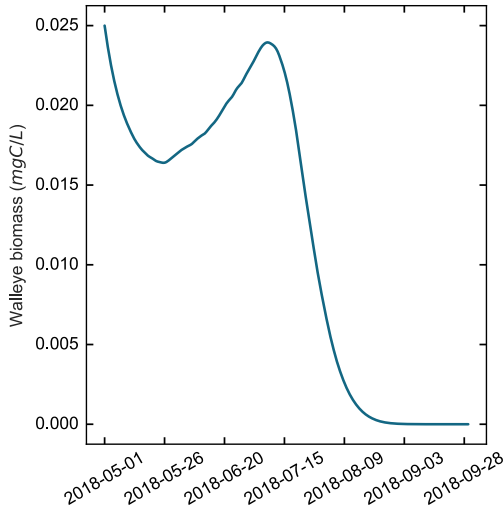


Figure 11: Predicted walleye biomass after fitting dynamical system model to data from Mendota lake, Wisconsin, United States, 2018.

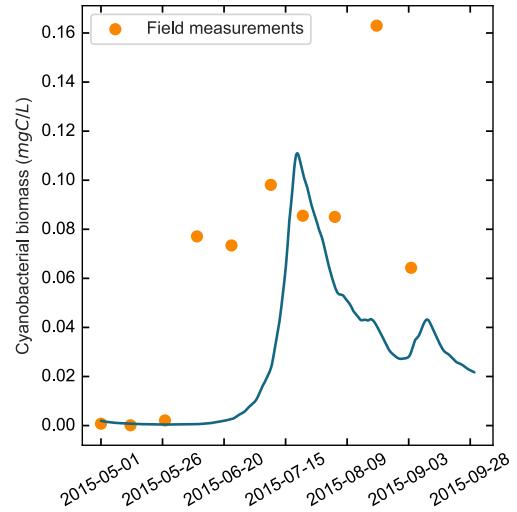


Figure 13: Predicted cyanobacterial biomass after fitting dynamical system model to data from Monona lake, Wisconsin, United States, 2015.

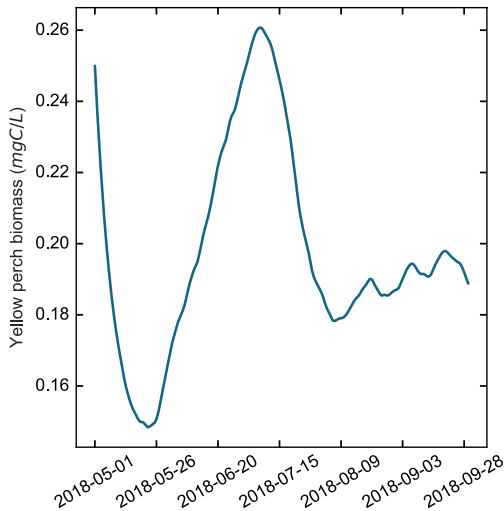


Figure 12: Predicted yellow perch biomass after fitting dynamical system model to data from Mendota lake, Wisconsin, United States, 2018.

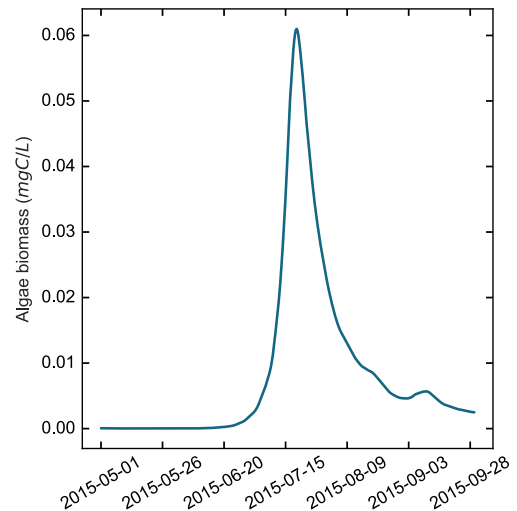


Figure 14: Predicted algal biomass after fitting dynamical system model to data from Monona lake, Wisconsin, United States, 2015.

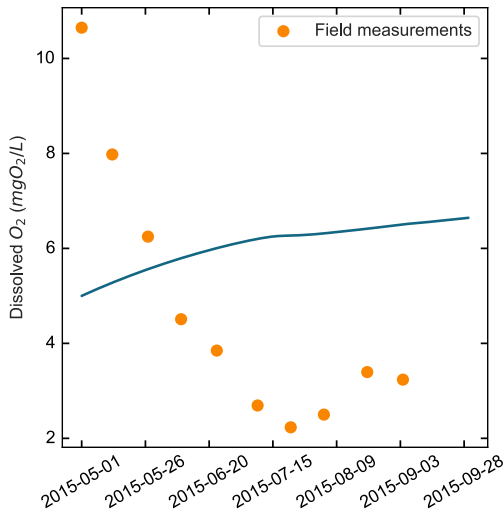


Figure 15: Satellite data for dissolved lake oxygen from Monona lake, Wisconsin, United States, 2015.

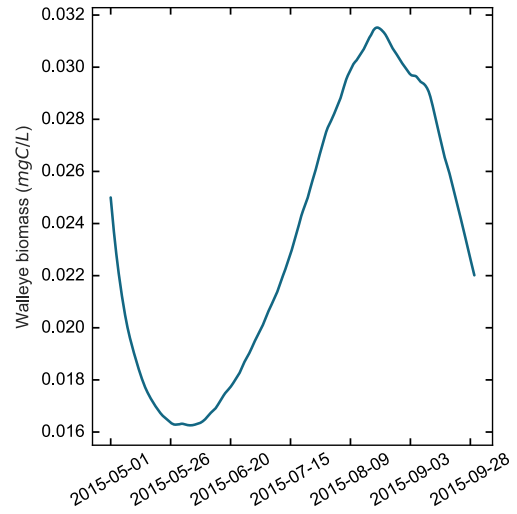


Figure 17: Predicted walleye biomass after fitting dynamical system model to data from Monona lake, Wisconsin, United States, 2015.

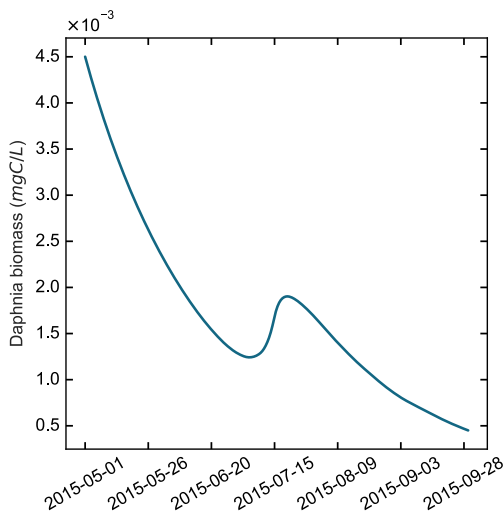


Figure 16: Predicted daphnia biomass after fitting dynamical system model to data from Monona lake, Wisconsin, United States, 2015.

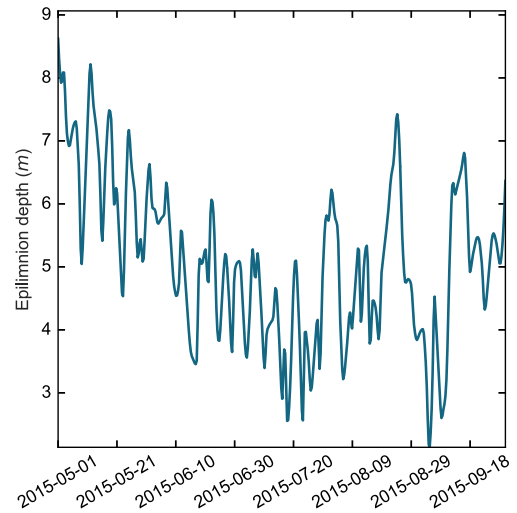


Figure 18: Satellite data for epilimnion depth from Monona lake, Wisconsin, United States, 2015.

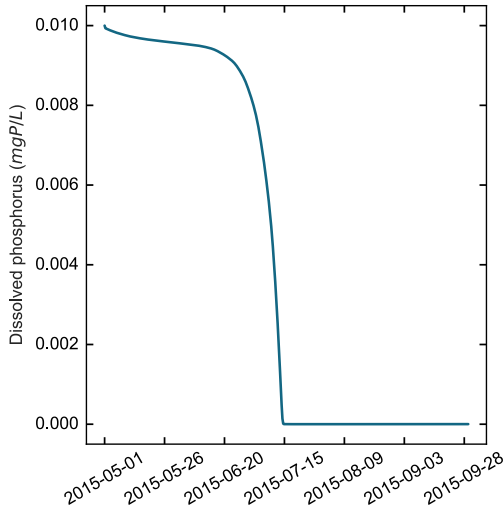


Figure 19: Predicted dissolved phosphorus concentration after fitting dynamical system model to data from Monona lake, Wisconsin, United States, 2015.

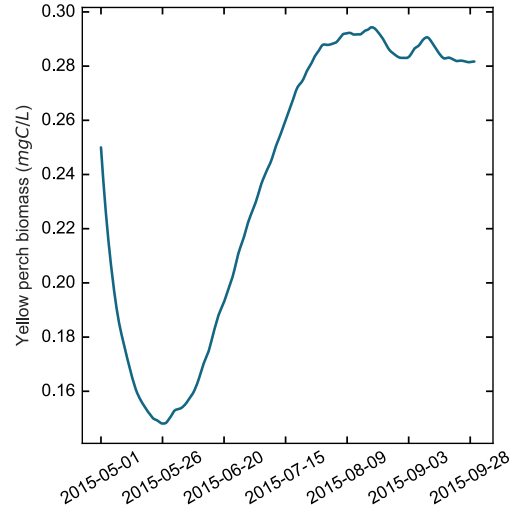


Figure 21: Predicted yellow perch biomass after fitting dynamical system model to data from Monona lake, Wisconsin, United States, 2015.

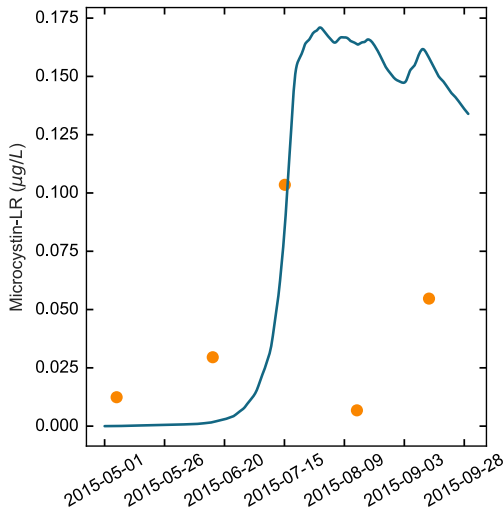


Figure 20: Predicted MC-LR concentration after fitting dynamical system model to data from Monona lake, Wisconsin, United States, 2015.

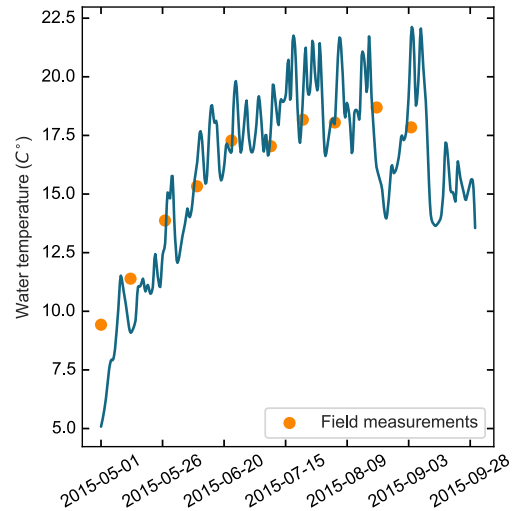


Figure 22: Annual prediction for cyanobacteria after fitting dynamical system model to data from Pigeon lake, Alberta, Canada in 2021.

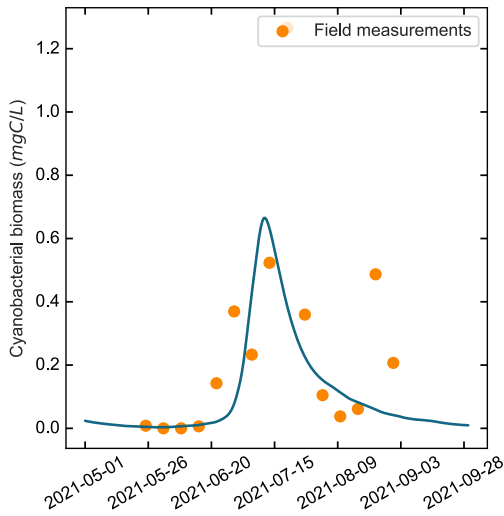


Figure 23: Predicted cyanobacterial biomass after fitting dynamical system model to data from Pigeon lake, Alberta, Canada, 2021.

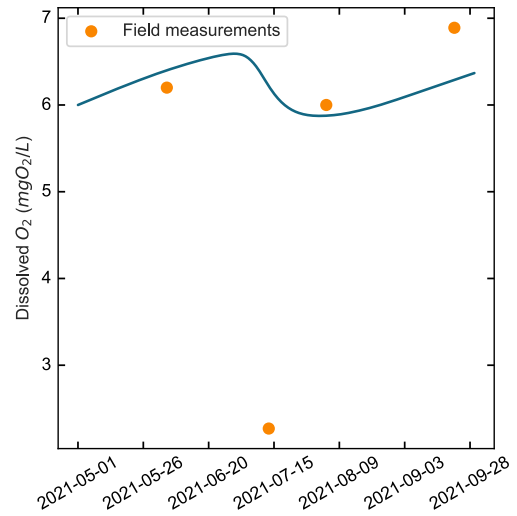


Figure 25: Satellite data for dissolved lake oxygen from Pigeon lake, Alberta, Canada, 2021.

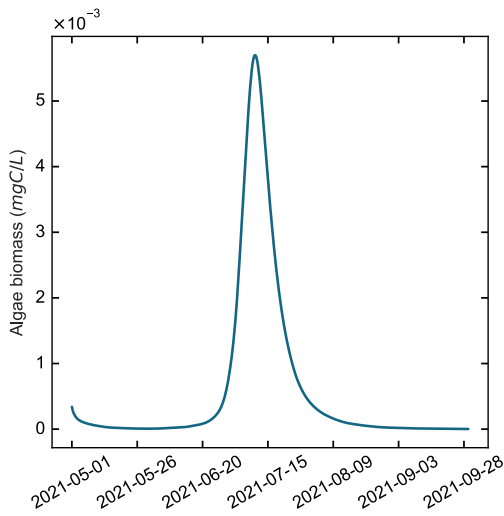


Figure 24: Predicted algal biomass after fitting dynamical system model to data from Pigeon lake, Alberta, Canada, 2021.

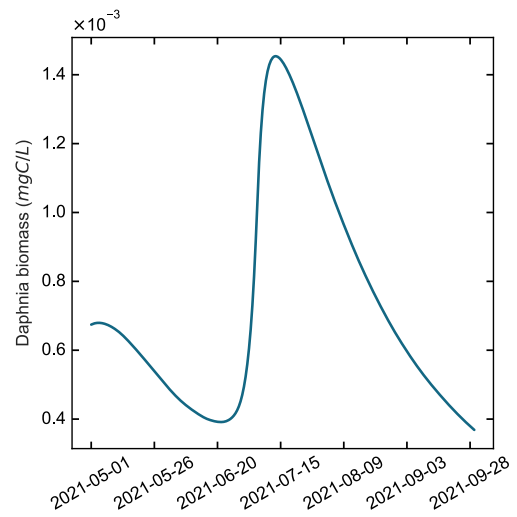


Figure 26: Predicted daphnia biomass after fitting dynamical system model to data from Pigeon lake, Alberta, Canada, 2021.

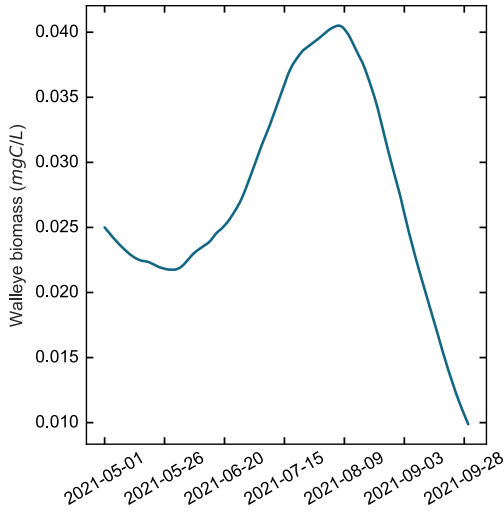


Figure 27: Predicted walleye biomass after fitting dynamical system model to data from Pigeon lake, Alberta, Canada, 2021.

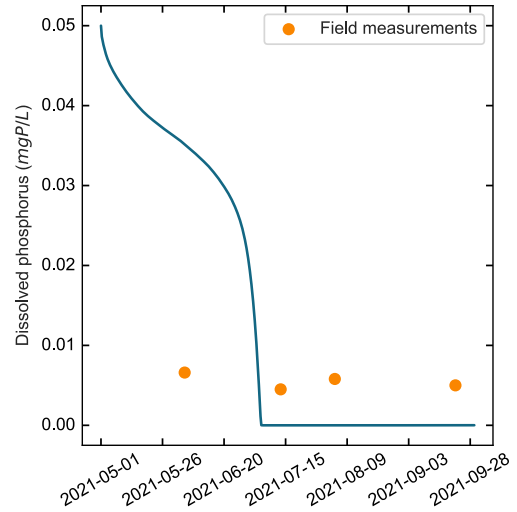


Figure 29: Predicted phosphorus concentration after fitting dynamical system model to data from Pigeon lake, Alberta, Canada, 2021.

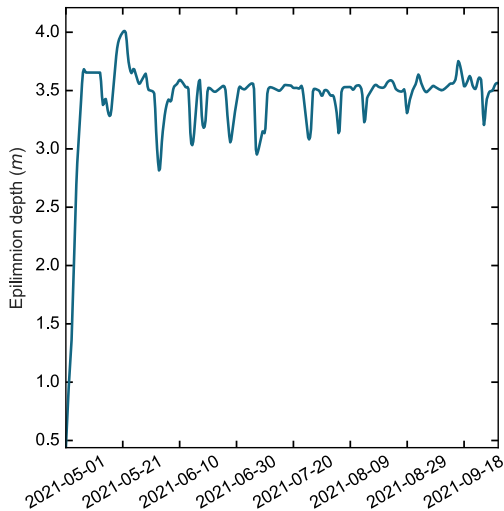


Figure 28: Satellite data for epilimnion depth from Pigeon lake, Alberta, Canada, 2021.

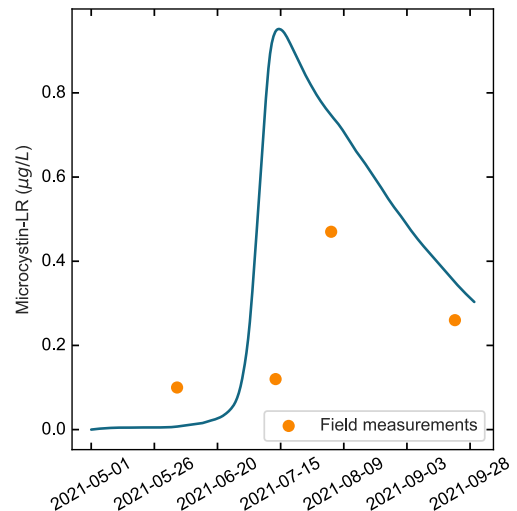


Figure 30: Predicted MC-LR concentration after fitting dynamical system model to data from Pigeon lake, Alberta, Canada, 2021.

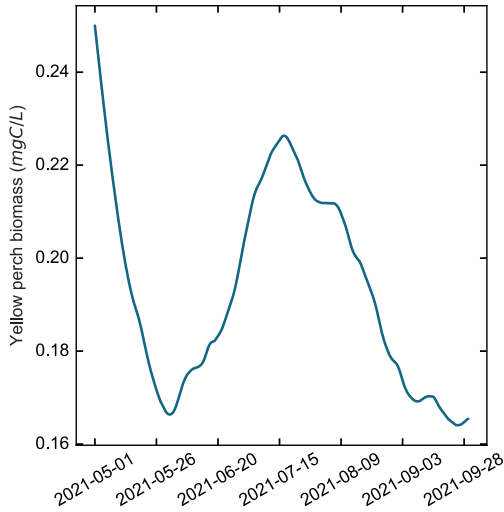


Figure 31: Predicted yellow perch biomass after fitting dynamical system model to data from Pigeon lake, Alberta, Canada, 2021.

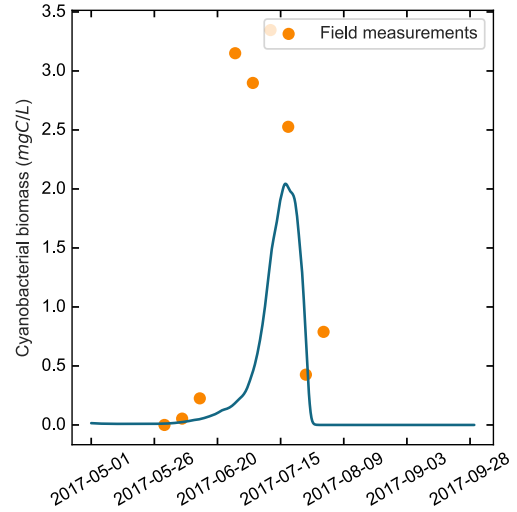


Figure 33: Predicted cyanobacterial biomass after fitting dynamical system model to data from Pine lake, Alberta, Canada, 2017.

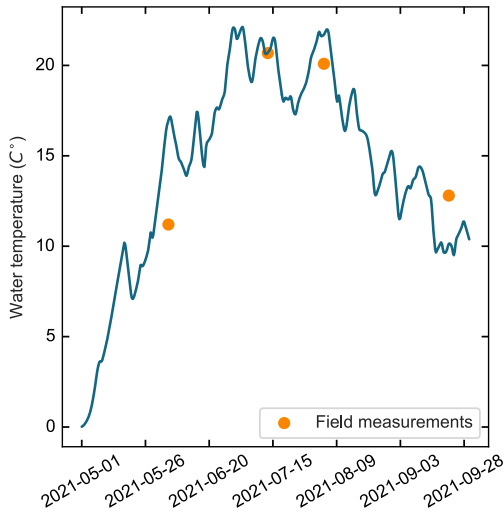


Figure 32: Satellite data for water temperature from Pigeon lake, Alberta, Canada, 2021.

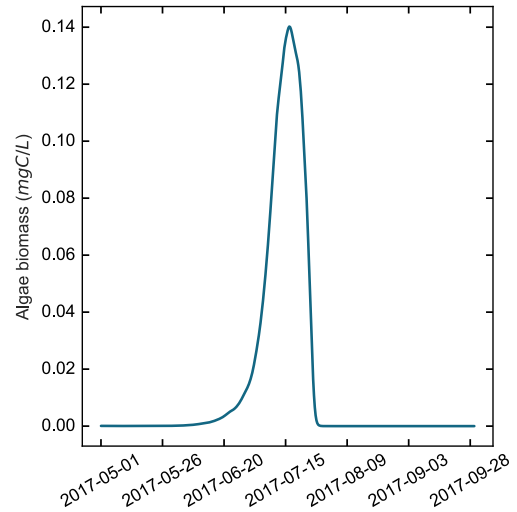


Figure 34: Predicted algal biomass after fitting dynamical system model to data from Pine lake, Alberta, Canada, 2017.

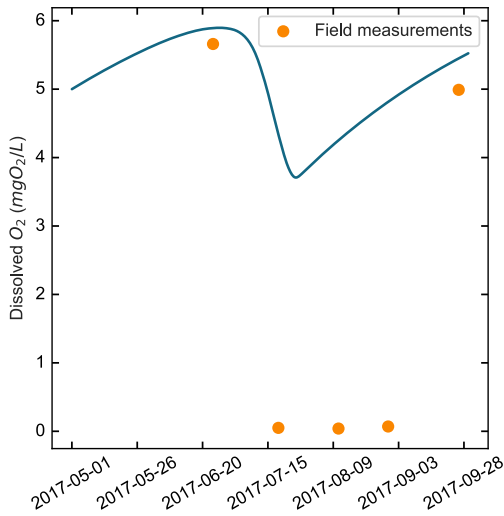


Figure 35: Satellite data for dissolved lake oxygen from Pine lake, Alberta, Canada, 2017.

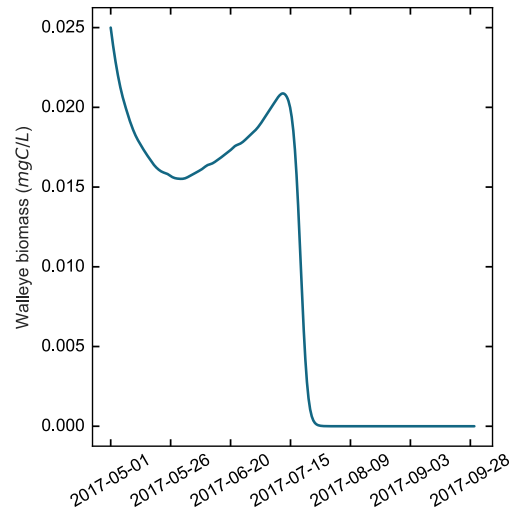


Figure 37: Predicted walleye biomass after fitting dynamical system model to data from Pine lake, Alberta, Canada, 2017.

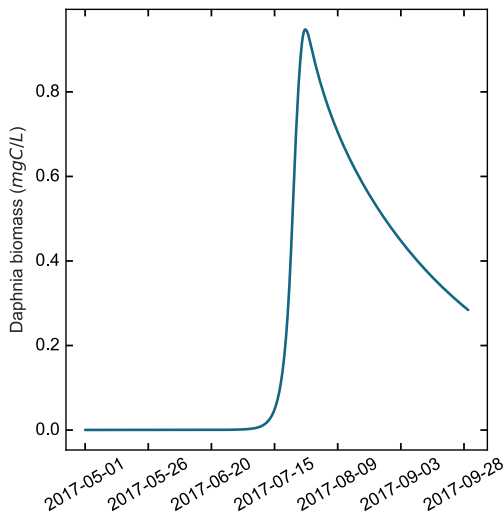


Figure 36: Predicted daphnia biomass after fitting dynamical system model to data from Pine lake, Alberta, Canada, 2017.

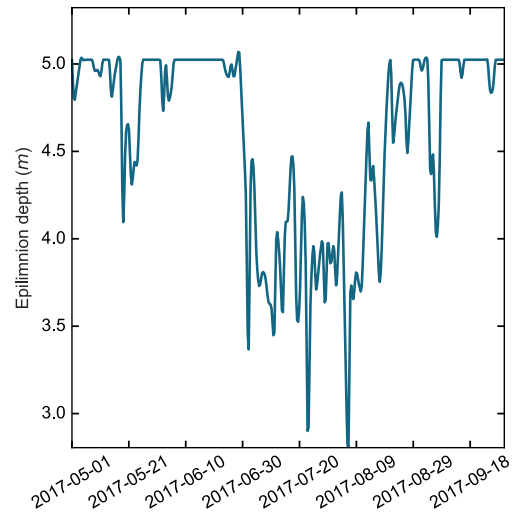


Figure 38: Satellite data for epilimnion depth from Pine lake, Alberta, Canada, 2017.



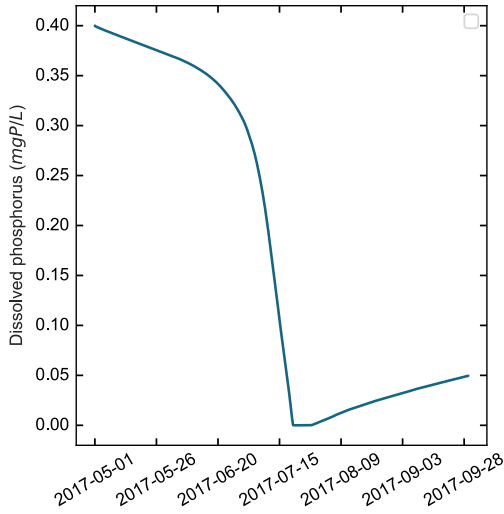


Figure 39: Predicted dissolved phosphorus concentration after fitting dynamical system model to data from Pine lake, Alberta, Canada, 2017.

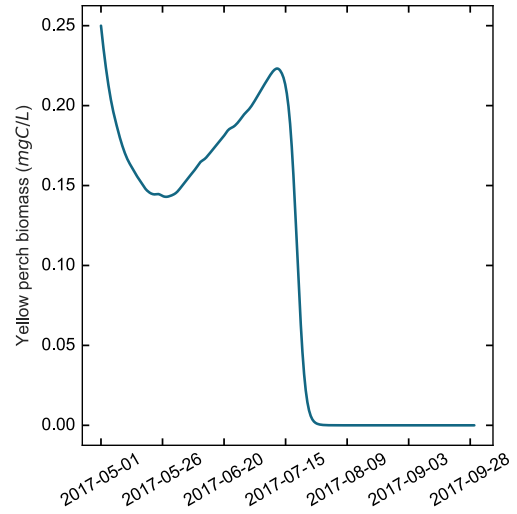


Figure 41: Predicted yellow perch biomass after fitting dynamical system model to data from Pine lake, Alberta, Canada, 2017.

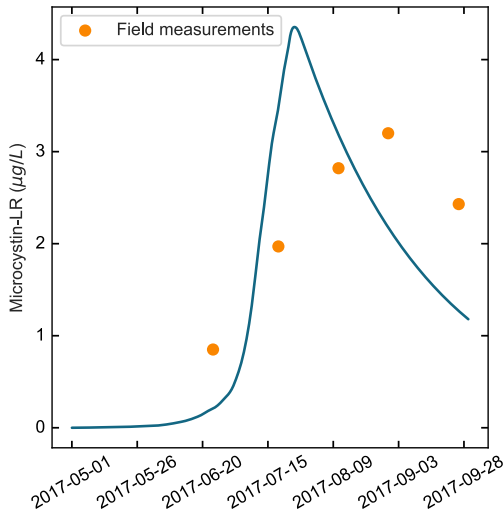


Figure 40: Predicted MC-LR concentration after fitting dynamical system model to data from Pine lake, Alberta, Canada, 2017.

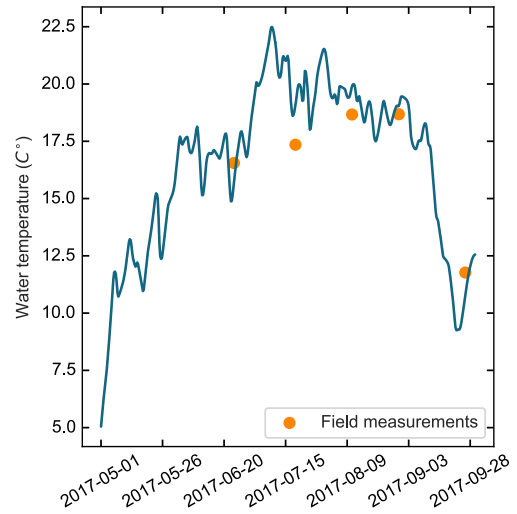


Figure 42: Satellite data for water temperature from Pine lake, Alberta, Canada, 2017.

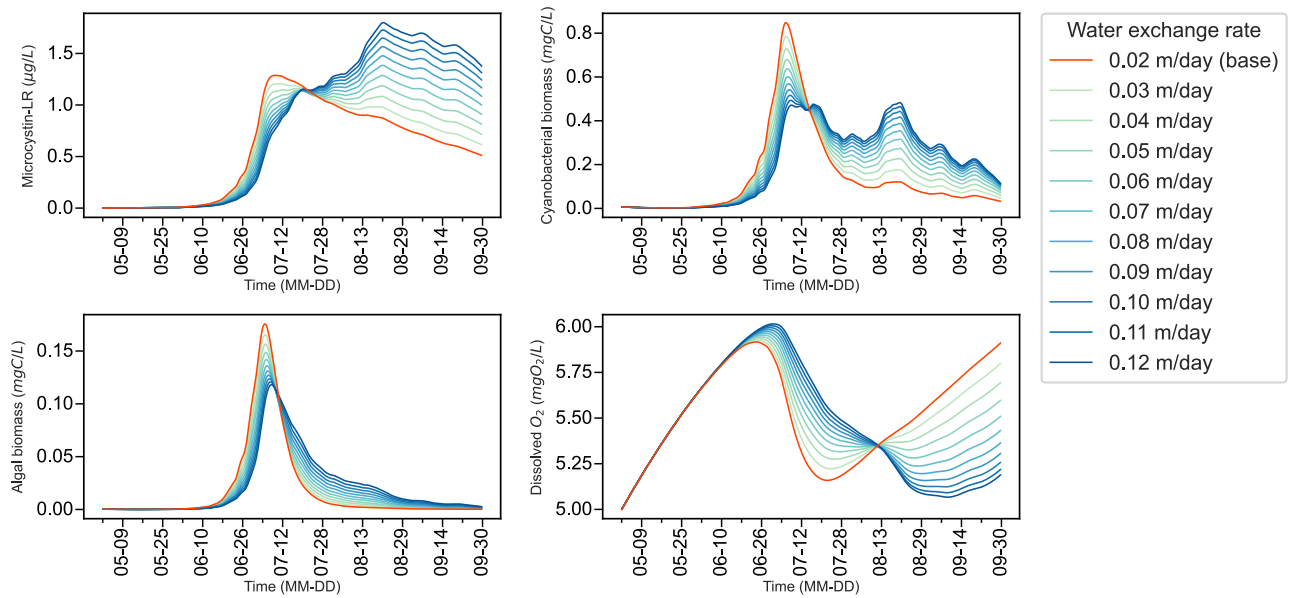


Figure 43: Impact of water exchange rate on various ecosystem metrics in Mendota lake (2018). The plots illustrate time series of MC-LR concentration, cyanobacterial biomass, algal biomass, and dissolved oxygen concentration, for different initial phosphorus values compared to baseline conditions.

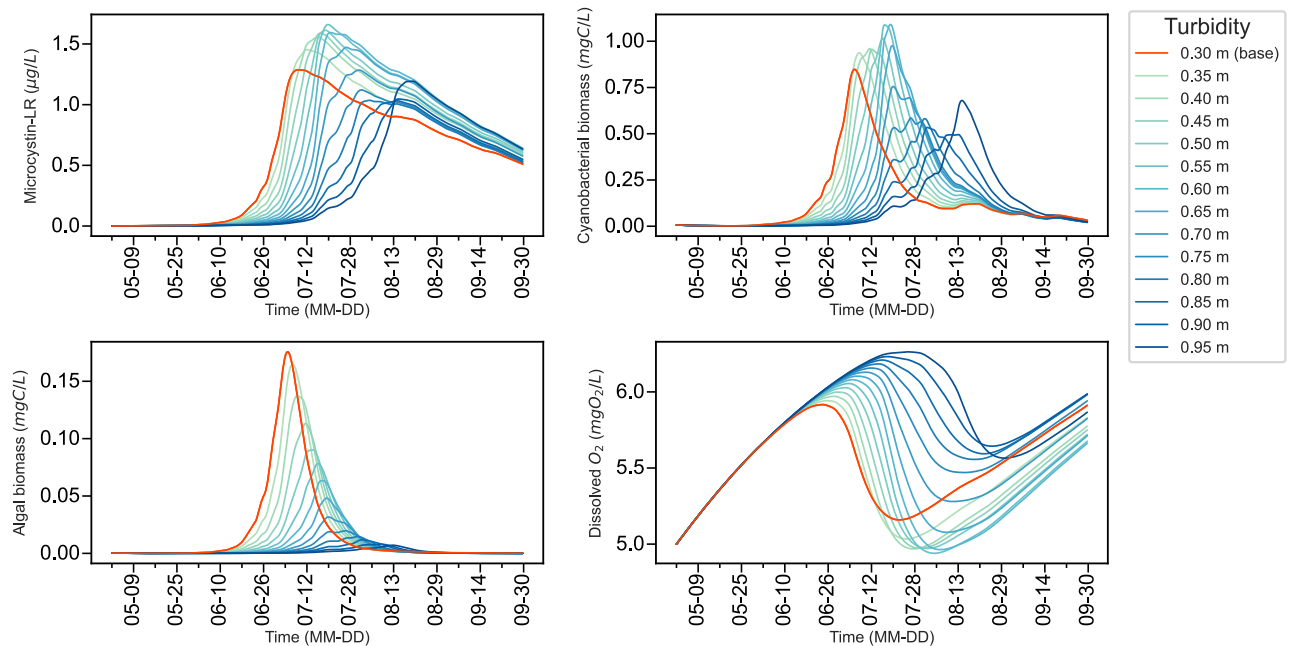


Figure 44: Impact of background light attenuation on various ecosystem metrics in Mendota lake (2018). The plots illustrate time series of MC-LR concentration, cyanobacterial biomass, algal biomass, and dissolved oxygen concentration, for different initial phosphorus values compared to baseline conditions.

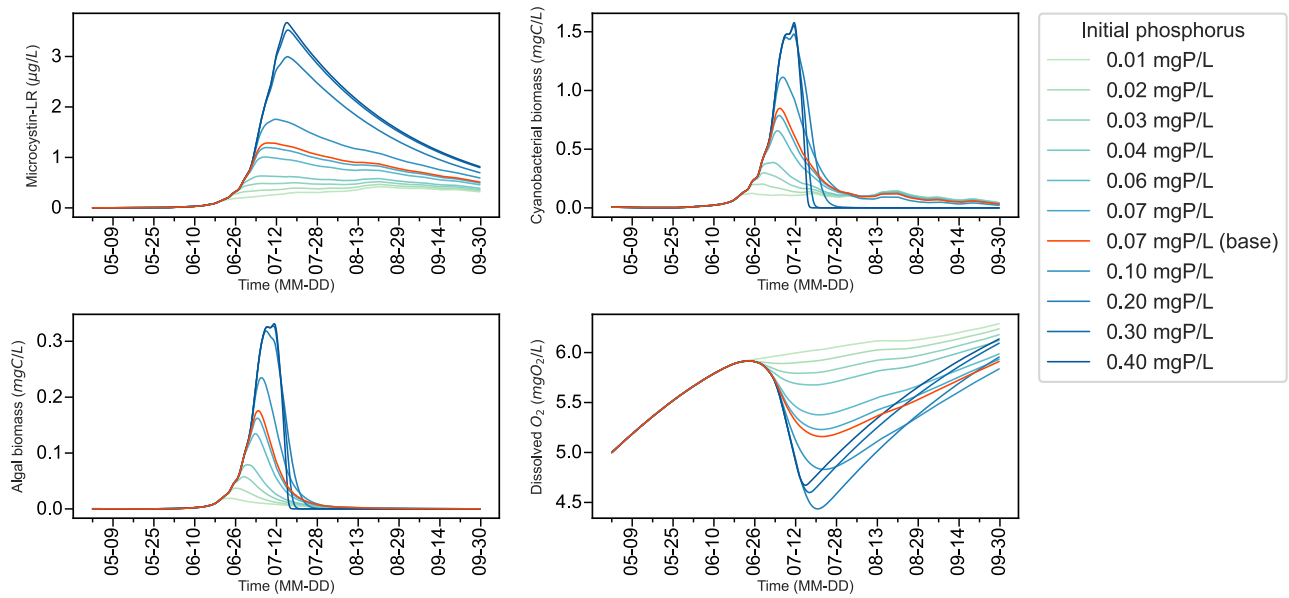


Figure 45: Impact of initial phosphorus on various ecosystem metrics in Mendota lake (2018). The plots illustrate time series of MC-LR concentration, cyanobacterial biomass, algal biomass, and dissolved oxygen concentration, for different initial phosphorus values compared to baseline conditions.

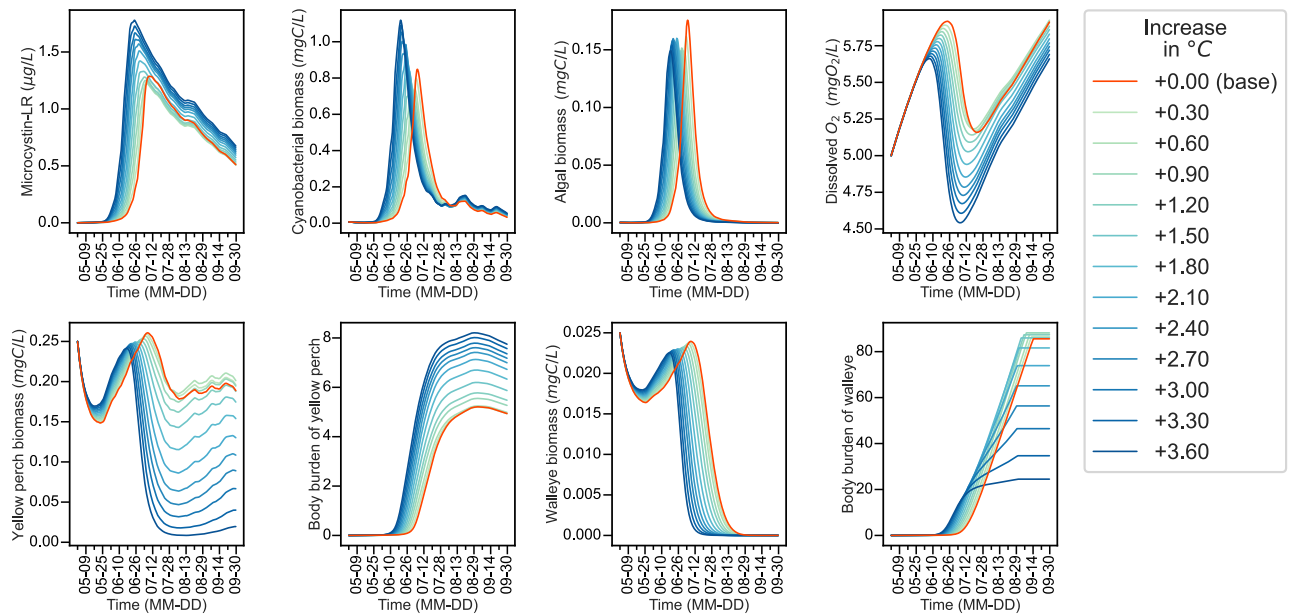


Figure 46: Impacts of temperature increases concentrated during the warm season (May to September 2018) on various ecosystem metrics in Mendota lake. The plots illustrate time series of MC-LR concentration, cyanobacterial biomass, algal biomass, dissolved oxygen concentration, yellow perch biomass, and walleye biomass, and walleye and yellow perch body burden, for different temperature values compared to present conditions (+0.0°C, in red).

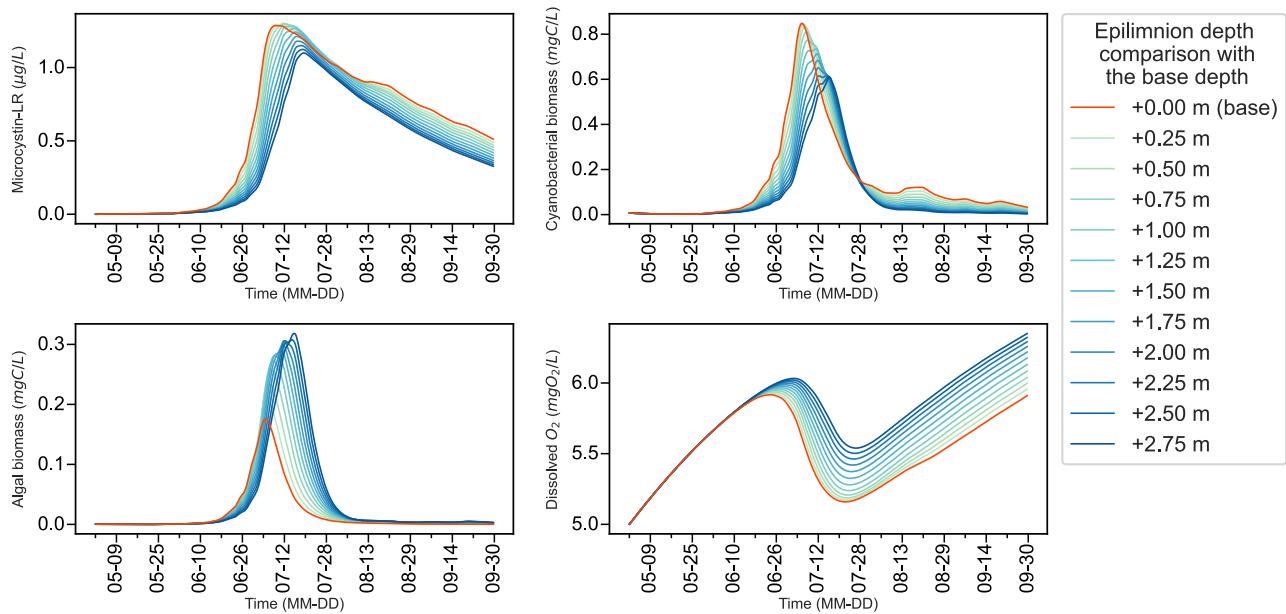


Figure 47: Impact of epilimnion depth on various ecosystem metrics in Mendota lake (2018). The plots illustrate time series of MC-LR concentration, cyanobacterial biomass, algal biomass, and dissolved oxygen concentration, for different initial phosphorus values compared to baseline conditions.

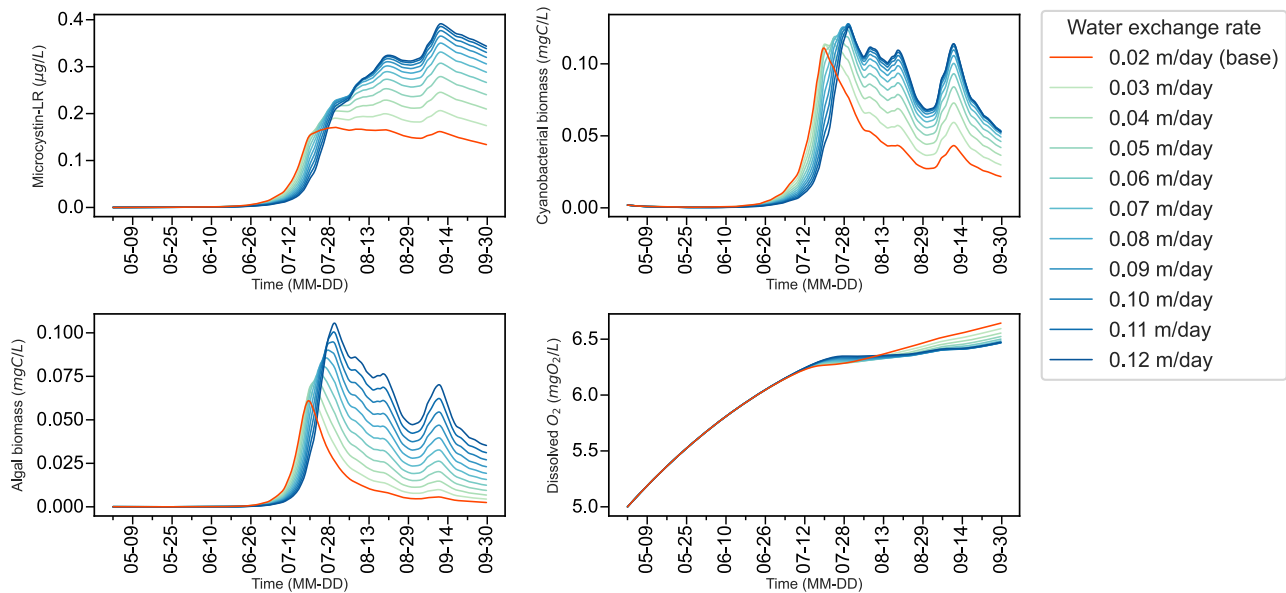


Figure 48: Impact of water exchange rate on various ecosystem metrics in Monona lake (2015). The plots illustrate time series of MC-LR concentration, cyanobacterial biomass, algal biomass, and dissolved oxygen concentration, for different initial phosphorus values compared to baseline conditions.

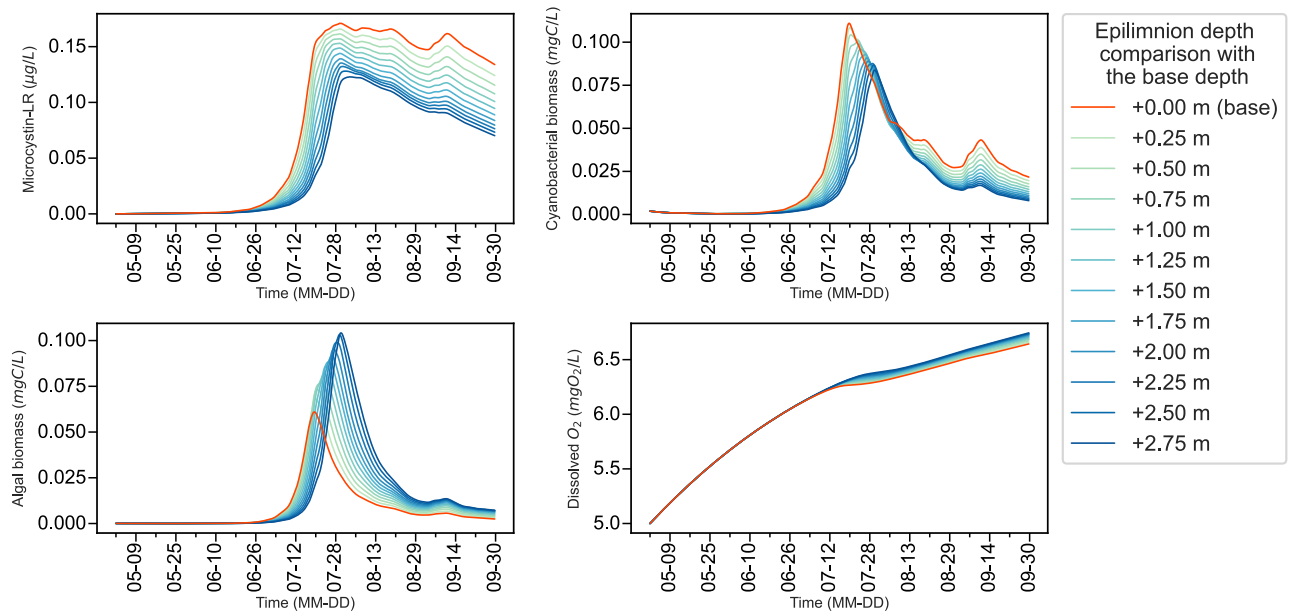


Figure 49: Impact of epilimnion depth on various ecosystem metrics in Monona lake (2015). The plots illustrate time series of MC-LR concentration, cyanobacterial biomass, algal biomass, and dissolved oxygen concentration, for different initial phosphorus values compared to baseline conditions.

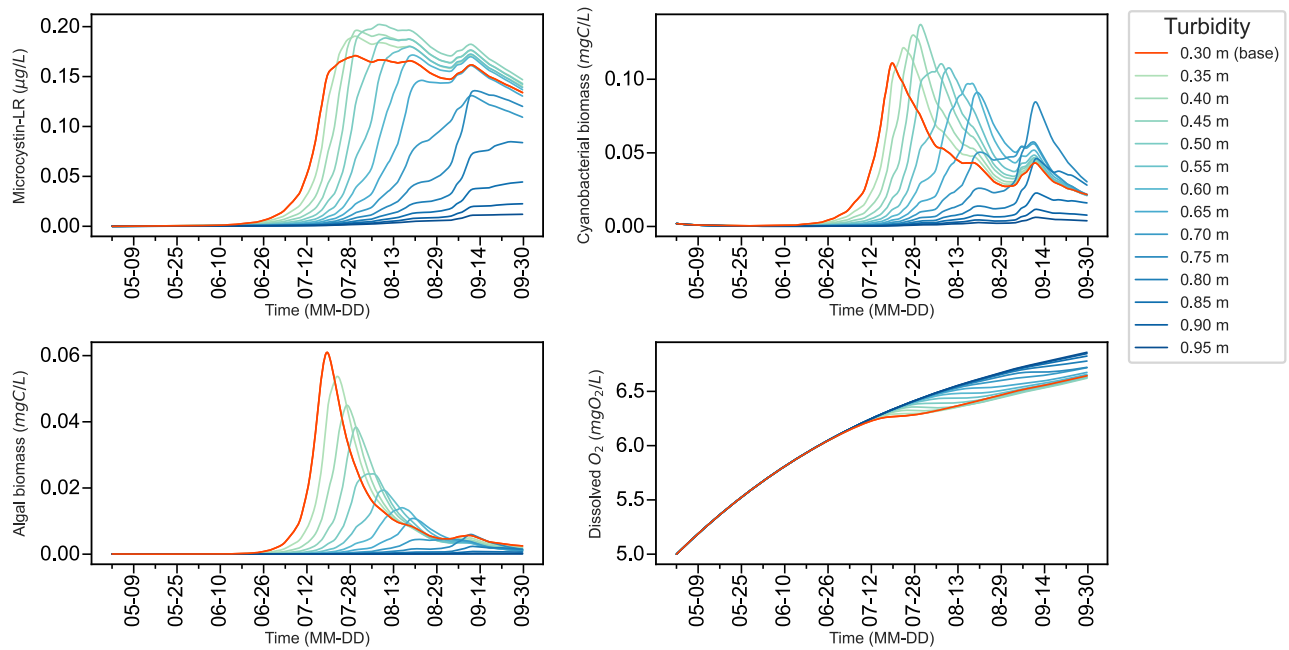


Figure 50: Impact of background light attenuation on various ecosystem metrics in Monona lake (2015). The plots illustrate time series of MC-LR concentration, cyanobacterial biomass, algal biomass, and dissolved oxygen concentration, for different initial phosphorus values compared to baseline conditions.

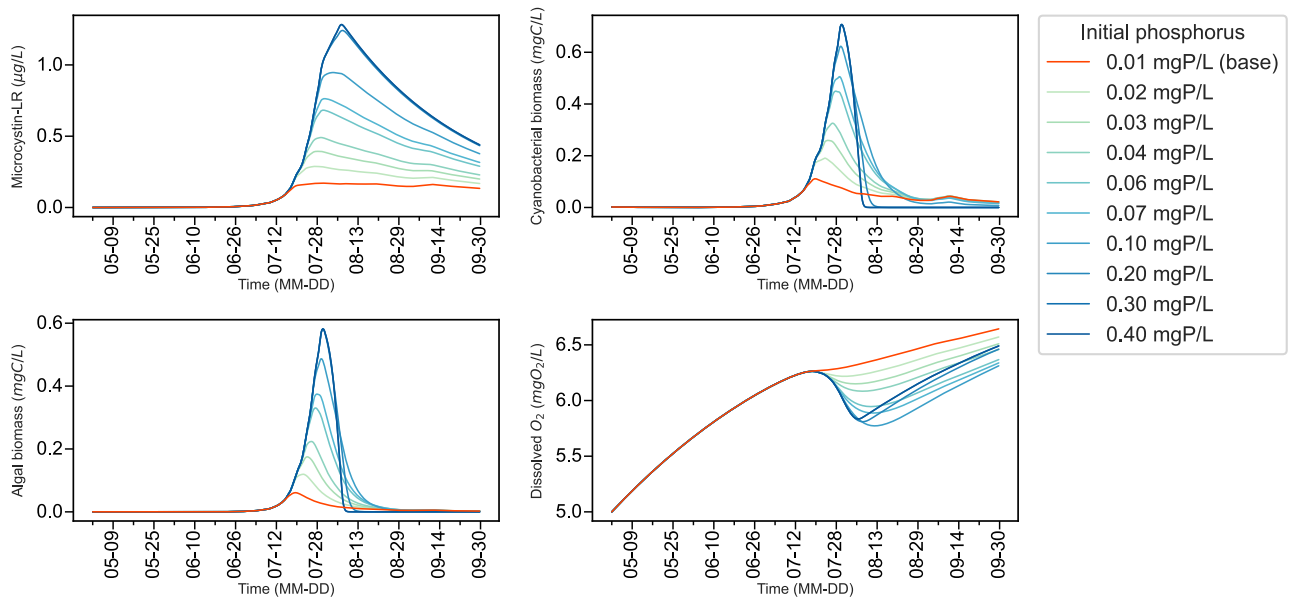


Figure 51: Impact of initial phosphorus on various ecosystem metrics in Monona lake (2015). The plots illustrate time series of MC-LR concentration, cyanobacterial biomass, algal biomass, and dissolved oxygen concentration, for different initial phosphorus values compared to baseline conditions.

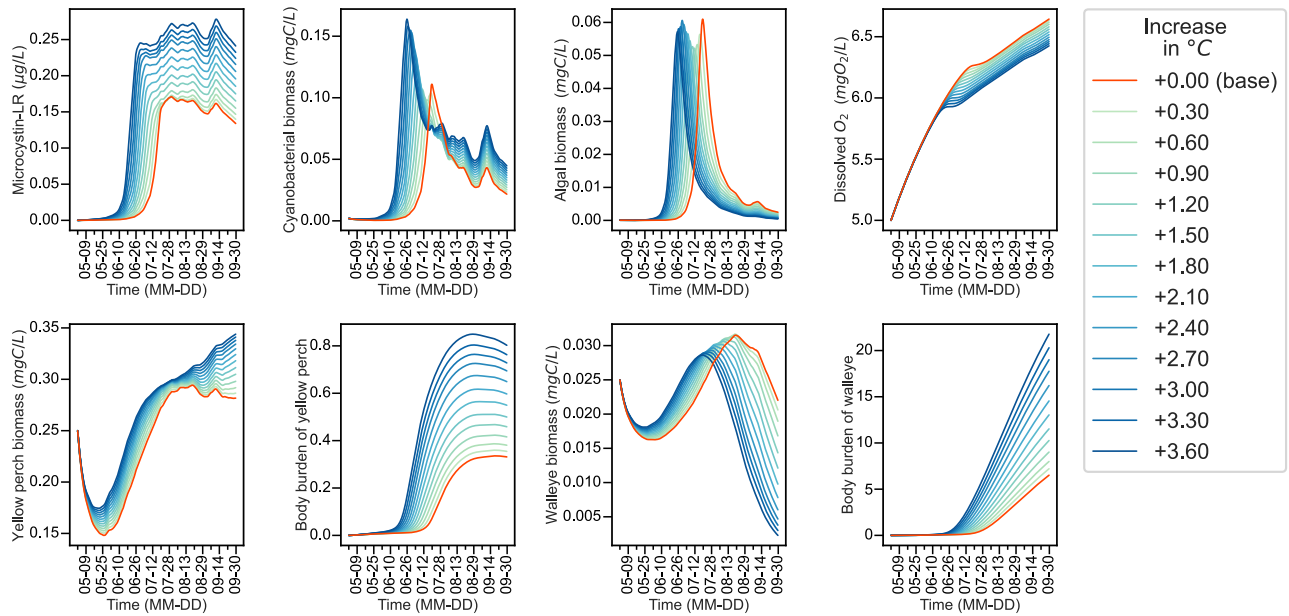


Figure 52: Impacts of temperature increases concentrated during the warm season (May to September 2015) on various ecosystem metrics in Monona lake. The plots illustrate time series of MC-LR concentration, cyanobacterial biomass, algal biomass, dissolved oxygen concentration, yellow perch biomass, and walleye biomass, and walleye and yellow perch body burden, for different temperature values compared to present conditions (+0.0°C, in red).

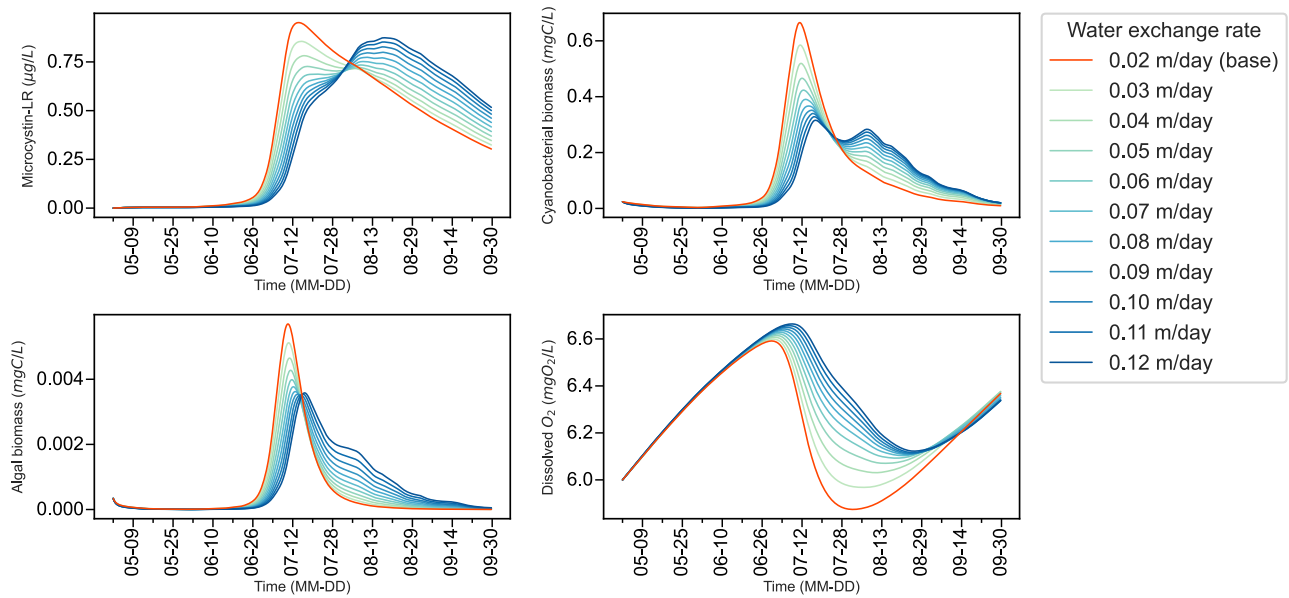


Figure 53: Impact of water exchange rate on various ecosystem metrics in Pigeon lake (2021). The plots illustrate time series of MC-LR concentration, cyanobacterial biomass, algal biomass, and dissolved oxygen concentration, for different initial phosphorus values compared to baseline conditions.

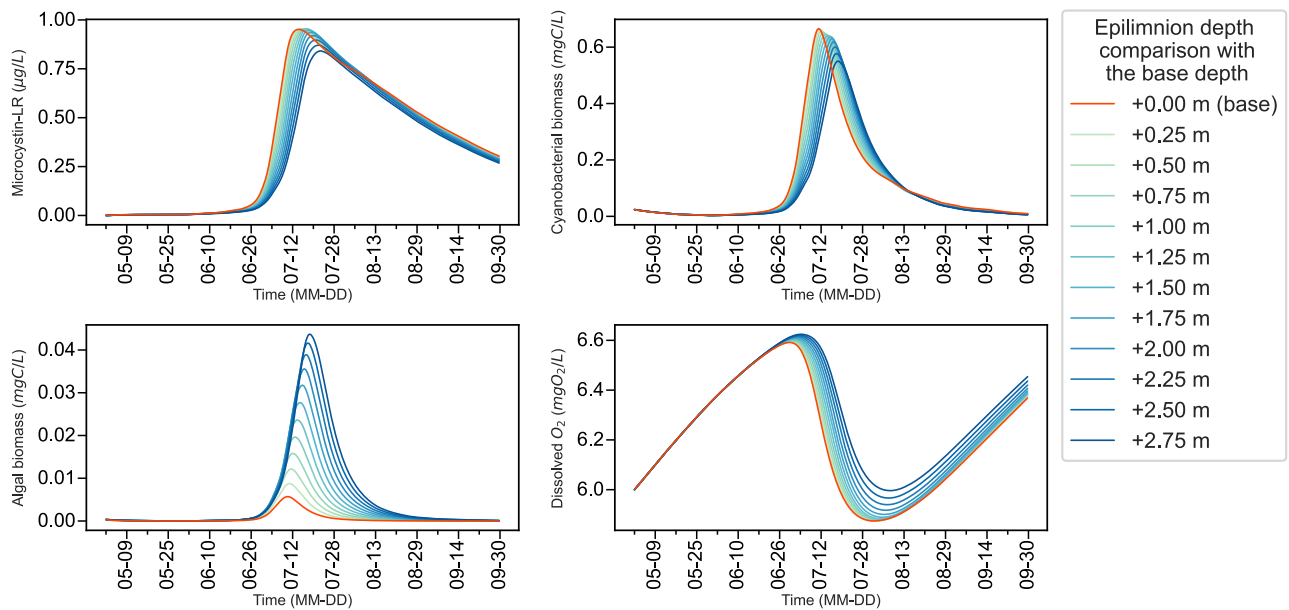


Figure 54: Impact of epilimnion depth on various ecosystem metrics in Pigeon lake (2021). The plots illustrate time series of MC-LR concentration, cyanobacterial biomass, algal biomass, and dissolved oxygen concentration, for different initial phosphorus values compared to baseline conditions.

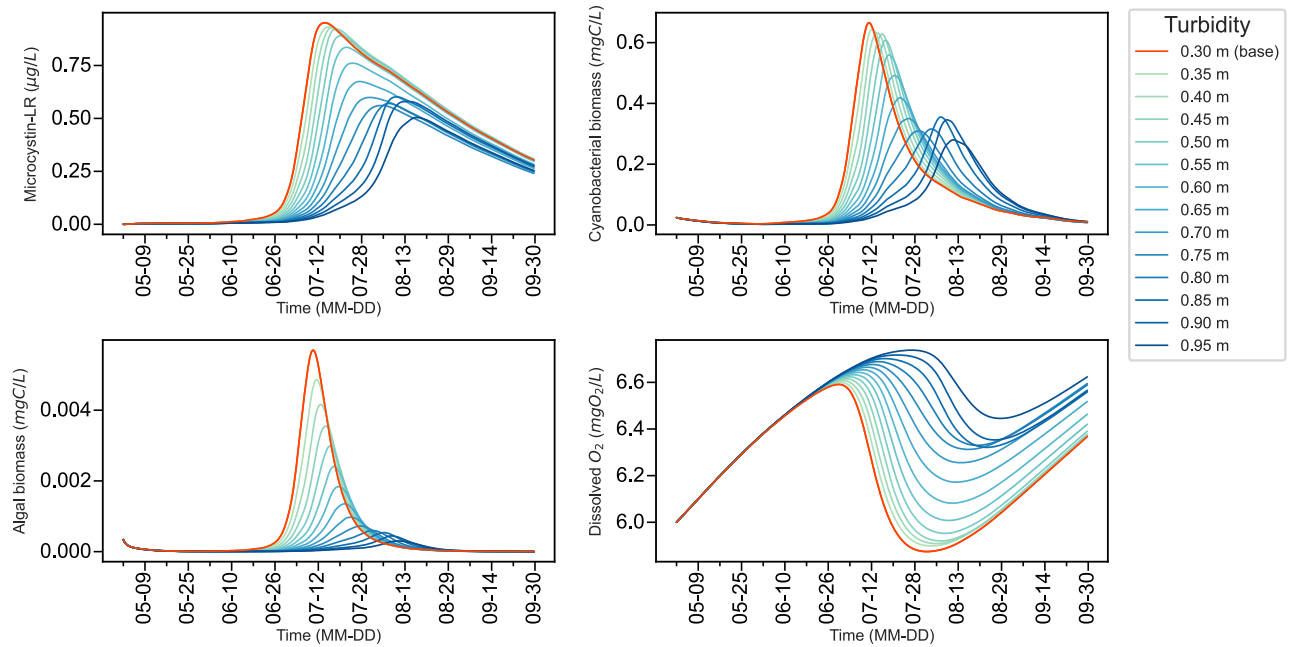


Figure 55: Impact of background light attenuation on various ecosystem metrics in Pigeon lake (2021). The plots illustrate time series of MC-LR concentration, cyanobacterial biomass, algal biomass, and dissolved oxygen concentration, for different initial phosphorus values compared to baseline conditions.

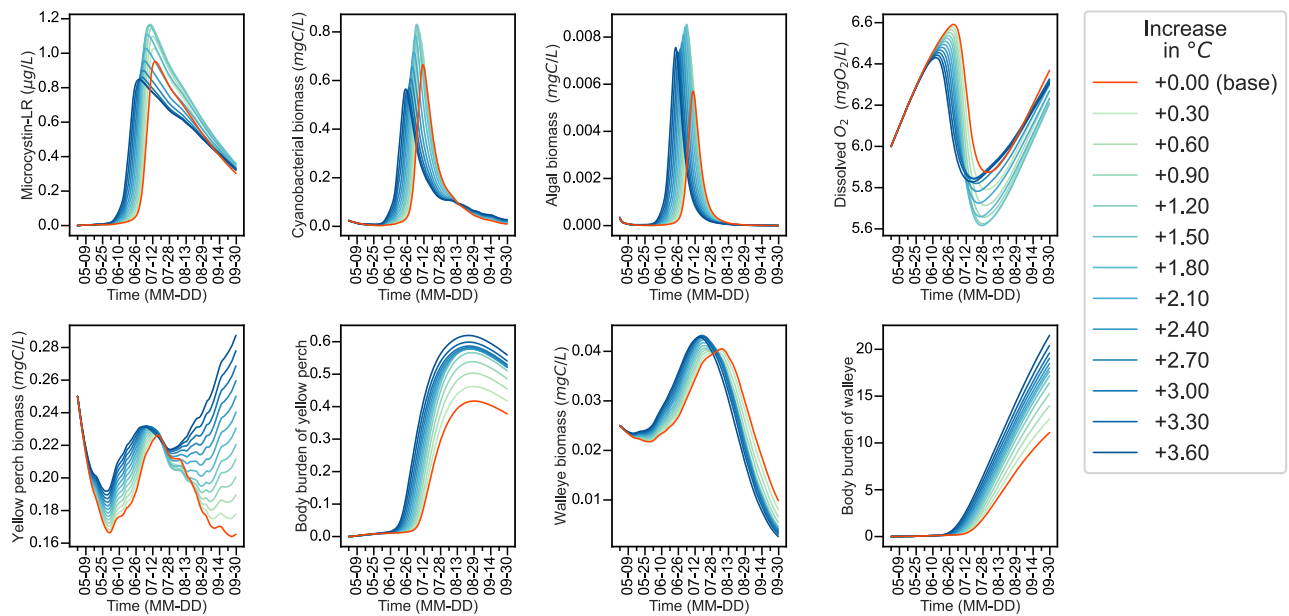


Figure 56: Impacts of temperature increases concentrated during the warm season (May to September 2021) on various ecosystem metrics in Pigeon lake. The plots illustrate time series of MC-LR concentration, cyanobacterial biomass, algal biomass, dissolved oxygen concentration, yellow perch biomass, and walleye biomass, and walleye and yellow perch body burden, for different temperature values compared to present conditions (+0.0°C, in red).



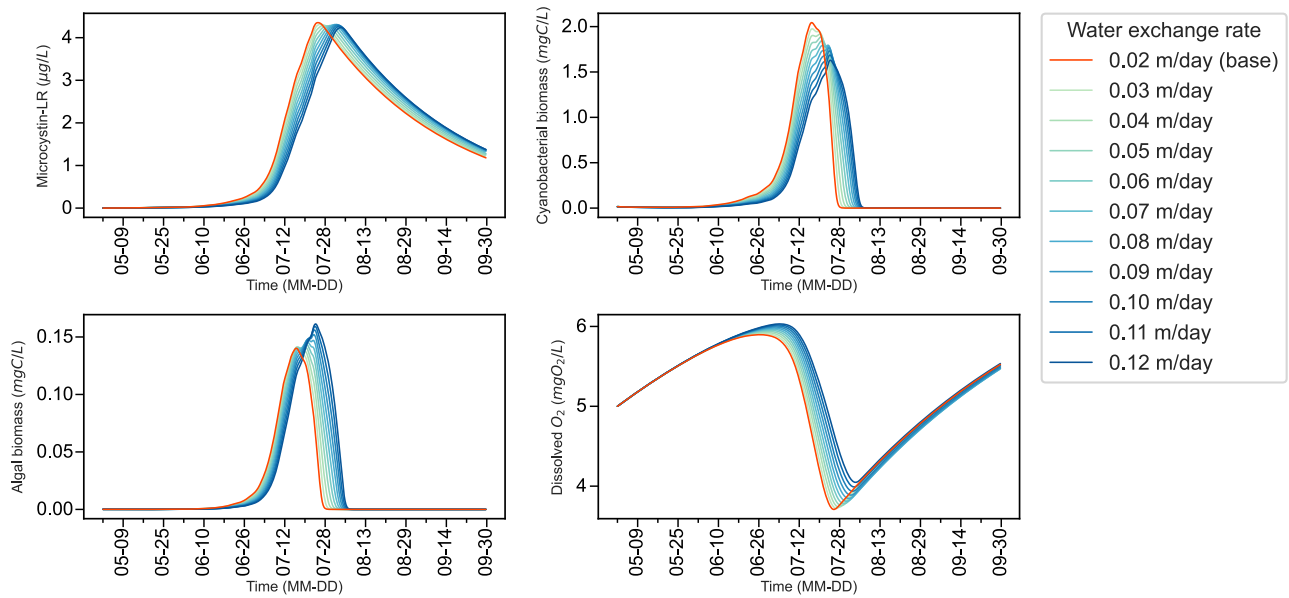


Figure 57: Impact of water exchange rate on various ecosystem metrics in Pine lake (2017). The plots illustrate time series of MC-LR concentration, cyanobacterial biomass, algal biomass, and dissolved oxygen concentration, for different initial phosphorus values compared to baseline conditions.

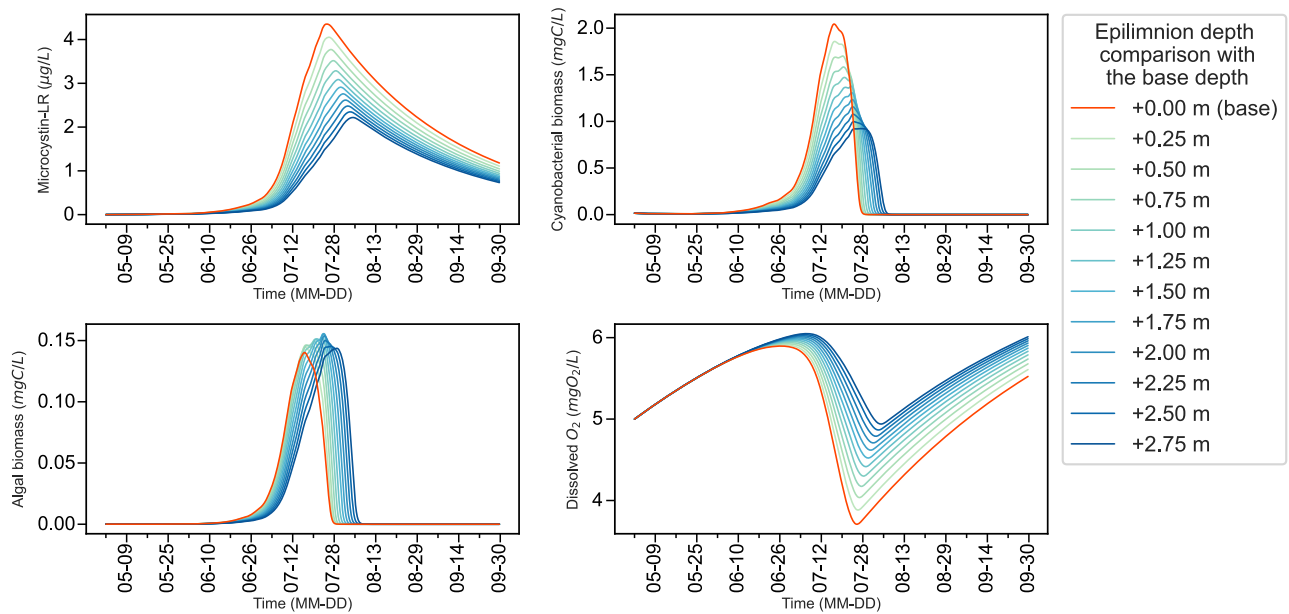


Figure 58: Impact of epilimnion depth on various ecosystem metrics in Pine lake (2017). The plots illustrate time series of MC-LR concentration, cyanobacterial biomass, algal biomass, and dissolved oxygen concentration, for different initial phosphorus values compared to baseline conditions.

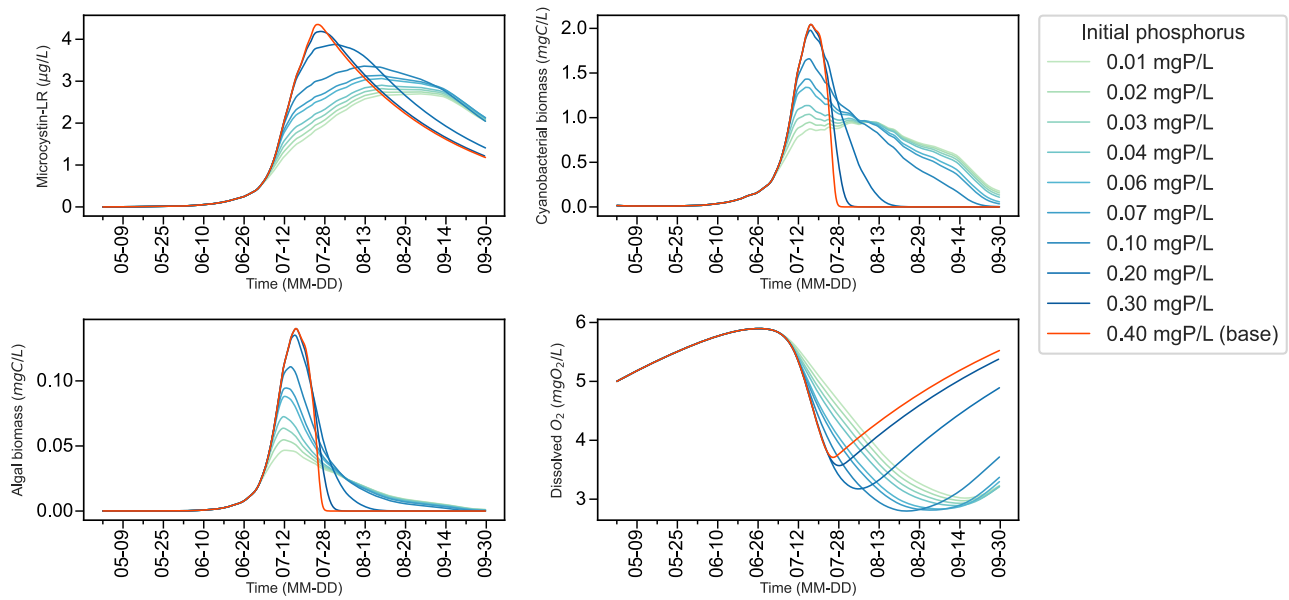


Figure 59: Impact of initial phosphorus on various ecosystem metrics in Pine lake (2017). The plots illustrate time series of MC-LR concentration, cyanobacterial biomass, algal biomass, and dissolved oxygen concentration, for different initial phosphorus values compared to baseline conditions.

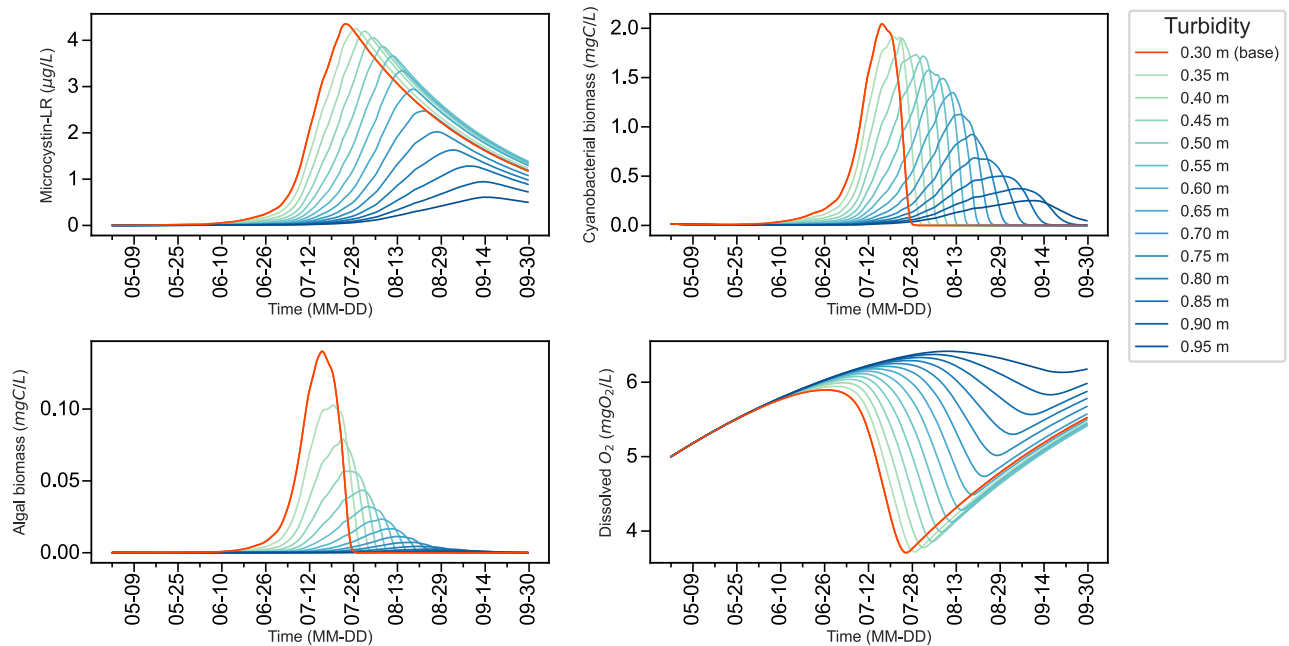


Figure 60: Impact of background light attenuation on various ecosystem metrics in Pine lake (2017). The plots illustrate time series of MC-LR concentration, cyanobacterial biomass, algal biomass, and dissolved oxygen concentration, for different initial phosphorus values compared to baseline conditions.

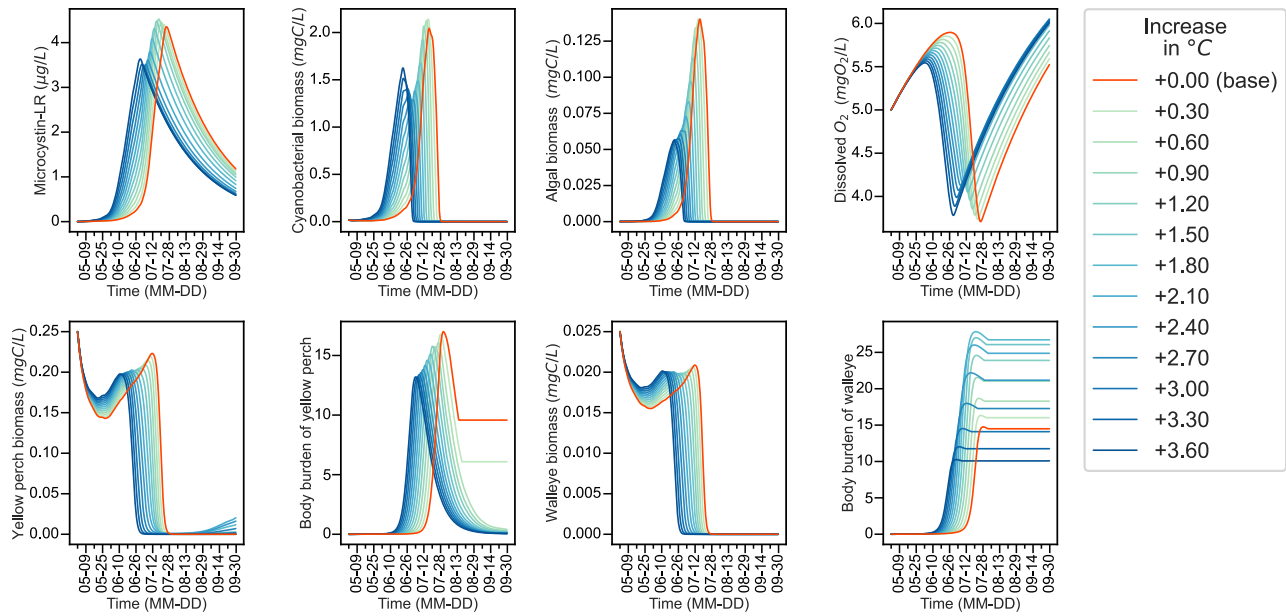


Figure 61: Impacts of temperature increases concentrated during the warm season (May to September 2017) on various ecosystem metrics in Pine lake. The plots illustrate time series of MC-LR concentration, cyanobacterial biomass, algal biomass, dissolved oxygen concentration, yellow perch biomass, and walleye biomass, and walleye and yellow perch body burden, for different temperature values compared to present conditions (+0.0°C, in red).

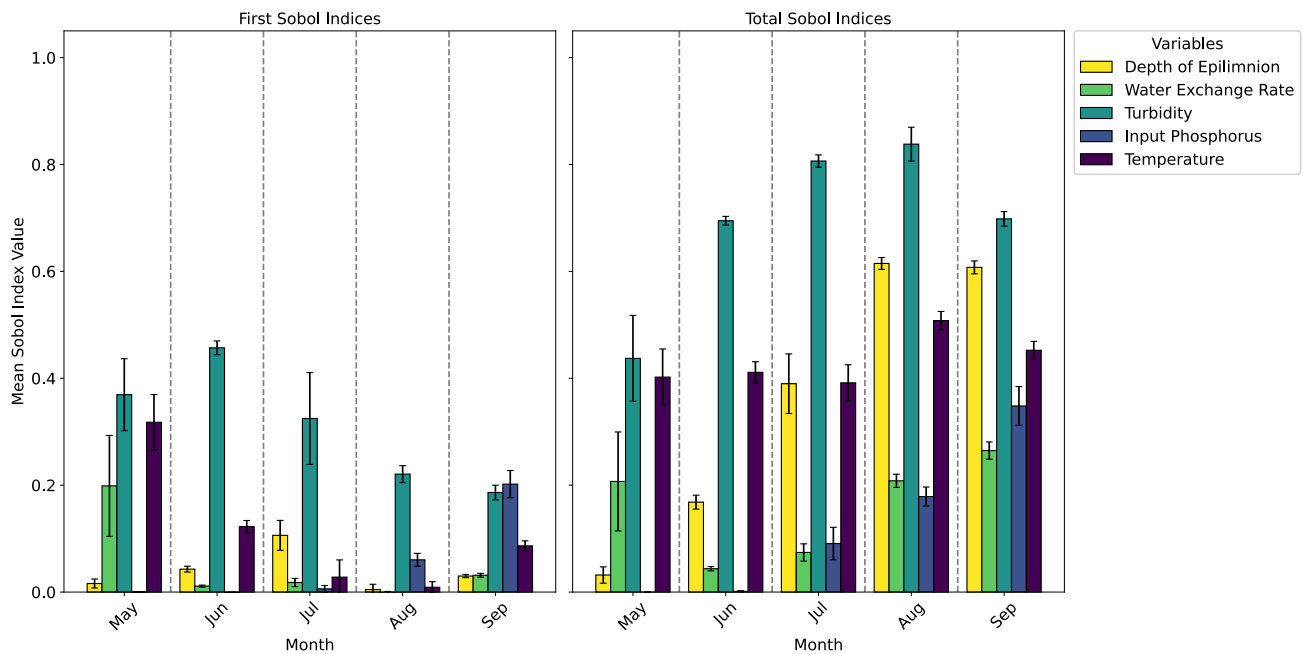


Figure 62: First-order (left) and total-order (right) Sobol indices for six model features: epilimnion depth, water exchange rate, turbidity, input and initial phosphorus, and water temperature, in Mendota lake, 2018. These indices vary each feature and calculate their direct (first-order) and combined direct and indirect (total-order) influence on cyanobacterial biomass.

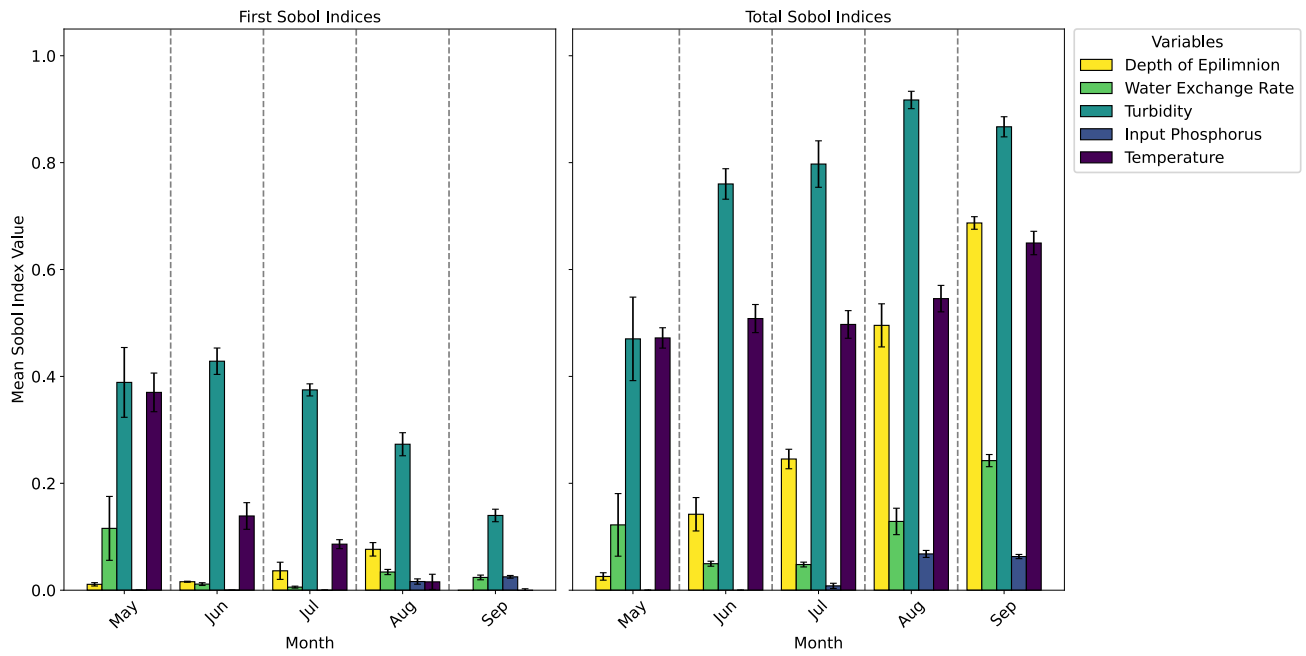


Figure 63: First-order (left) and total-order (right) Sobol indices for six model features: epilimnion depth, water exchange rate, turbidity, input and initial phosphorus, and water temperature, in Monona lake, 2015. These indices vary each feature and calculate their direct (first-order) and combined direct and indirect (total-order) influence on cyanobacterial biomass.

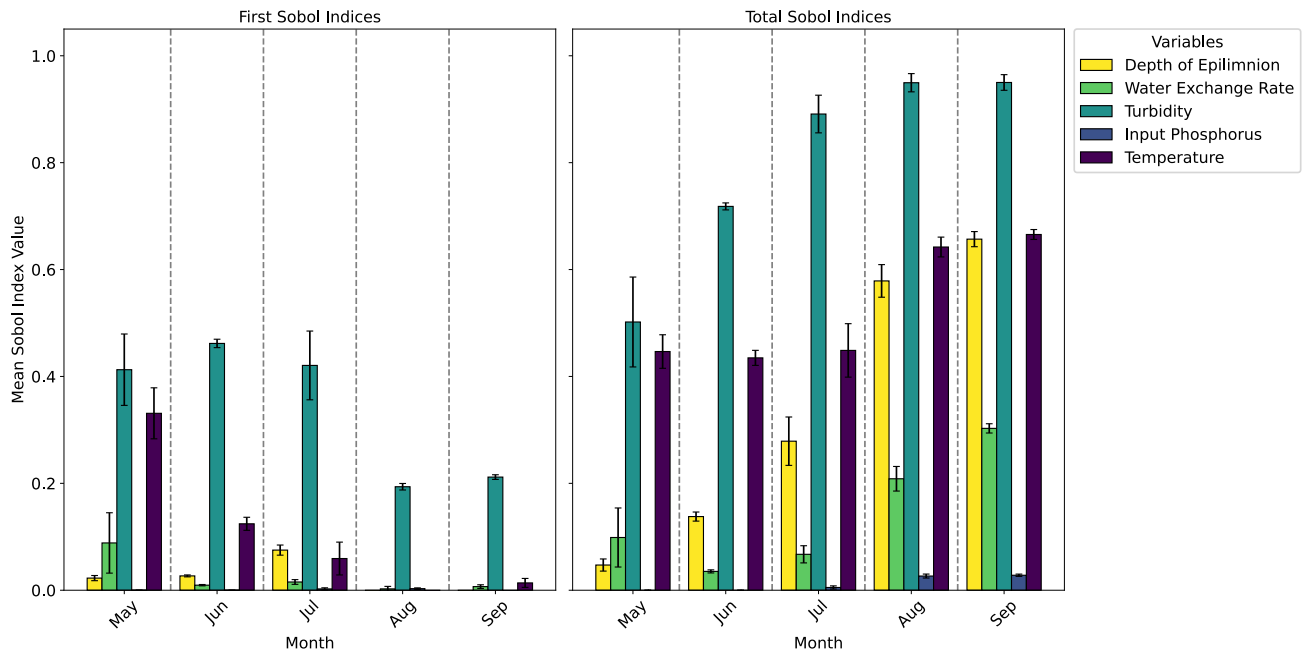


Figure 64: First-order (left) and total-order (right) Sobol indices for six model features: epilimnion depth, water exchange rate, turbidity, input and initial phosphorus, and water temperature, in Pine lake, 2017. These indices vary each feature and calculate their direct (first-order) and combined direct and indirect (total-order) influence on cyanobacterial biomass.

Table 1: State variables and their respective meanings and units used in the model.

Variable	Meaning	Unit
$M$	concentration of MC-LR	$\mu\text{g/L}$
$B$	concentration of cyanobacterial biomass	$\text{mgC/L}$
$A$	concentration of algal biomass	$\text{mgC/L}$
$Y$	concentration of yellow perch biomass	$\text{mgC/L}$
$W$	concentration of walleye biomass	$\text{mgC/L}$
$D$	concentration of daphnia biomass	$\text{mgC/L}$
$Q_B$	cyanobacterial cell quota	$\text{gP/gC}$
$Q_A$	algal cell quota	$\text{gP/gC}$
$v_A$	body burden of MC-LR on algae	$\mu\text{g/L/mgC/L}$
$v_D$	body burden of MC-LR on daphnia	$\mu\text{g/L/mgC/L}$
$v_Y$	body burden of MC-LR on yellow perch	$\mu\text{g/L/mgC/L}$
$v_W$	body burden of MC-LR on walleye	$\mu\text{g/L/mgC/L}$
$P$	dissolved mineral phosphorus concentration	$\text{mgP/L}$
$O$	dissolved oxygen concentration	$\text{mgO}_2/\text{L}$

Table 2: The hypercube that defines the bounded conditions for the greedy algorithm.

Parameter	Min. Value	Max. Value	Min. Fitted Value	Max. Fitted Value
$\alpha_D$	0.001	0.01	0.0013	0.002
$\alpha_Y$	0.0001	0.013	0.0045	0.01
$\tau_D$	0.5	2	1.2	1.47
$\tau_Y$	0.5	2	1.08	1.47
$a_A$	0.001	0.1	0.042	0.074
$\sigma_A$	0.001	0.01	0.0031	0.0062
$x_A$	0.001	0.01	0.039	0.0098
$B(0)$	0	0.1	0.0015	0.23
$A(0)$	0	0.1	0.000057	0.0027
$D(0)$	0	0.1	0.0006	0.0045

Table 3: The full parameter table is downloadable as an excel file, named "parameter\_table.xlsx".

## References

- [1] H. Wang, H. L. Smith, Y. Kuang, and J. J. Elser, Dynamics of Stoichiometric Bacteria-Algae Interactions in the Epilimnion, *SIAM Journal on Applied Mathematics* **68**:pp. 503–522 2007
- [2] C. M. Heggerud, H. Wang, and M. A. Lewis, Transient Dynamics of a Stoichiometric Cyanobacteria Model via Multiple-Scale Analysis, *SIAM Journal on Applied Mathematics* **80**:pp. 1223–1246 2020
- [3] J. Huisman and F. J. Weissing, Light-Limited Growth and Competition for Light in Well-Mixed Aquatic Environments: An Elementary Model, *Ecology* **75**:pp. 507–520 1994
- [4] J. T. O. Kirk. *Light and Photosynthesis in Aquatic Ecosystems*. 3rd ed. Cambridge University Press, 2010.
- [5] S. Diehl, S. Berger, and R. Wöhrl, Flexible Nutrient Stoichiometry Mediates Environmental Influences on Phytoplankton and Its Resources, *Ecology* **86**:pp. 2931–2945 2005
- [6] E. M. Grima, F. G. Camacho, J. A. S. Pérez, J. M. F. Sevilla, F. G. A. Fernández, and A. C. Gómez, A Mathematical Model of Microalgal Growth in Light-Limited Chemostat Culture, *Journal of Chemical Technology & Biotechnology* **61**:pp. 167–173 1994
- [7] S. Aiba. “Growth Kinetics of Photosynthetic Microorganisms”. *Microbial Reactions*. Ed. by A. Fiechter, S. Aiba, B. Atkinson, et al. Berlin, Heidelberg: Springer Berlin Heidelberg, 1982, pp. 85–156.
- [8] P. H. C. Eilers and J. C. H. Peeters, Dynamic Behaviour of a Model for Photosynthesis and Photoinhibition, *Ecological Modelling* **69**:pp. 113–133 1993
- [9] M. R. Droop, Some thoughts on nutrient limitation in algae, *Journal of Phycology* **9**:pp. 264–272 1973
- [10] H. Wang, P. V. Garcia, S. Ahmed, and C. M. Heggerud, Mathematical comparison and empirical review of the Monod and Droop forms for resource-based population dynamics, *Ecological Modelling* **466**:p. 109887 2022
- [11] F. M. M. Morel, Kinetics of nutrient uptake and growth in phytoplankton, *Journal of Phycology* **23**:pp. 137–150 1987
- [12] L. Zhao and W. Huang, Models for identifying significant environmental factors associated with cyanobacterial bloom occurrence and for predicting cyanobacterial blooms, *Journal of Great Lakes Research* **40**:pp. 265–273 2014
- [13] Q. Huang, H. Wang, and M. A. Lewis, The impact of environmental toxins on predator–prey dynamics, *Journal of Theoretical Biology* **378**:pp. 12–30 2015
- [14] A. Peace and H. Wang, Compensatory Foraging in Stoichiometric Producer–Grazer Models, *Bulletin of Mathematical Biology* **81**: 2019
- [15] *FishBase Trophic Ecology - Perca flavescens*. <https://www.fishbase.se/TrophicEco/DietCompoList.php?ID=359&GenusName=Perca&SpeciesName=flavescens&fc=306&StockCode=373>. Accessed: Insert Date Here.
- [16] G. Hartman, A Biological Synopsis of Walleye (*Sander vitreus*), *Canadian Manuscript Report of Fisheries and Aquatic Sciences*:pp. 1–10 2009



- [17] S. Jähnichen, T. Ihle, and T. Petzoldt, Variability of microcystin cell quota: A small model explains dynamics and equilibria, *Limnologia* **38**:pp. 339–349 2008
- [18] J.-P. Descy et al., Identifying the factors determining blooms of cyanobacteria in a set of shallow lakes, *Ecological Informatics* **34**:pp. 129–138 2016
- [19] J.-F. Briand, C. Leboulanger, J.-F. Humbert, C. Bernard, and P. Dufour, *Cylindrospermopsis raciborskii* (cyanobacteria) invasion at mid-latitudes: Selection, wide physiological tolerance, or global warming? 1, *Journal of Phycology* **40**:pp. 231–238 2004
- [20] H. W. Paerl, N. S. Hall, and E. S. Calandrino, Controlling harmful cyanobacterial blooms in a world experiencing anthropogenic and climatic-induced change, *Science of the total environment* **409**:pp. 1739–1745 2011
- [21] H. W. Paerl and T. G. Otten, Harmful cyanobacterial blooms: causes, consequences, and controls, *Microbial ecology* **65**:pp. 995–1010 2013
- [22] L. Rosso, J. R. Lobry, and J.-P. Flandrois, An unexpected correlation between cardinal temperatures of microbial growth highlighted by a new model, *Journal of theoretical biology* **162**:pp. 447–463 1993
- [23] Y Le Marc, V Huchet, C. Bourgeois, J. Guyonnet, P Mafart, and D Thuault, Modelling the growth kinetics of *Listeria* as a function of temperature, pH and organic acid concentration, *International journal of food microbiology* **73**:pp. 219–237 2002
- [24] T. Ruiz, A.-m. Koussoroplis, M. Danger, J.-p. Aguer, N. Morel-Desrosiers, and A. Bec, U-shaped response Unifies views on temperature dependency of stoichiometric requirements, *Ecology Letters* **23**:pp. 860–869 2020
- [25] P. M. Yurista, Temperature-dependent energy budget of an Arctic Cladoceran, *Daphnia middendorffiana*, *Freshwater biology* **42**:pp. 21–34 1999
- [26] P. M. Yurista. *The effect of temperature on the biology of two Cladocerans*. University of Michigan, 1997.
- [27] R. M. Schoolfield, P. Sharpe, and C. E. Magnuson, Non-linear regression of biological temperature-dependent rate models based on absolute reaction-rate theory, *Journal of theoretical biology* **88**:pp. 719–731 1981
- [28] H. Huh, H. E. Calbert, and D. A. Stuiber, Effects of temperature and light on growth of yellow perch and walleye using formulated feed, *Transactions of the American Fisheries Society* **105**:pp. 254–258 1976
- [29] T. L. Galarowicz and D. H. Wahl, Differences in growth, consumption, and metabolism among walleyes from different latitudes, *Transactions of the American Fisheries Society* **132**:pp. 425–437 2003
- [30] M Bernreuther, J.-P. Herrmann, M. Peck, and A Temming, Growth energetics of juvenile herring, *C lupea harengus* L.: food conversion efficiency and temperature dependency of metabolic rate, *Journal of Applied Ichthyology* **29**:pp. 331–340 2013
- [31] R. Smith, A. Paul, and J. Paul, Effect of food intake and temperature on growth and conversion efficiency of juvenile walleye pollock (*Theragra chalcogramma* (Pallas)): a laboratory study, *ICES Journal of Marine Science* **42**:pp. 241–253 1986

- [32] M. Jobling, The influence of environmental temperature on growth and conversion efficiency in fish, *ICES CM* **4**: 1995
- [33] N. P. Lester, A. J. Dextrase, R. S. Kushneriuk, M. R. Rawson, and P. A. Ryan, Light and temperature: key factors affecting walleye abundance and production, *Transactions of the American Fisheries Society* **133**:pp. 588–605 2004
- [34] S. D. Hart, D. L. Garling, J. A. Malison, et al. *Yellow Perch (Perca flavescens) Culture Guide*. Culture Series. North Central Regional Aquaculture Center in cooperation with USDA, 2006.
- [35] K. E. Hokanson, Temperature requirements of some percids and adaptations to the seasonal temperature cycle, *Journal of the Fisheries Board of Canada* **34**:pp. 1524–1550 1977
- [36] J. Shukla, A. Misra, and P. Chandra, Modeling and analysis of the algal bloom in a lake caused by discharge of nutrients, *Applied Mathematics and Computation* **196**:pp. 782–790 2008
- [37] B. Hasan, M. S. Islam, P. Kundu, U. K. Mallick, et al., Modeling the Effects of Algal Bloom on Dissolved Oxygen in Eutrophic Water Bodies, *Journal of Mathematics* **2023**: 2023
- [38] A. Misra, Modeling the depletion of dissolved oxygen in a lake due to submerged macrophytes, *Nonlinear Analysis: Modelling and Control* **15**:pp. 185–198 2010
- [39] M. S. Pollock, L. M. J. Clarke, and M. G. Dubé, The effects of hypoxia on fishes: from ecological relevance to physiological effects, *Environ. Rev.* **15**:pp. 1–14 2007
- [40] Y. Mallya, The effects of dissolved oxygen on fish growth in aquaculture, United Nations University, *Fisheries Training Programme, UNU-FTP* **30**: 2007
- [41] Z. Wang et al., Hypoxia-induced physiological responses in fish: From organism to tissue to molecular levels, *Ecotoxicology and Environmental Safety* **267**:p. 115609 2023
- [42] J. Wang, D.-Q. Lu, B. Jiang, H.-L. Luo, G.-L. Lu, and A.-X. Li, The effect of intermittent hypoxia under different temperature on the immunomodulation in Streptococcus agalactiae vaccinated Nile tilapia (*Oreochromis niloticus*), *Fish & shellfish immunology* **79**:pp. 181–192 2018
- [43] B. M. Long, G. J. Jones, and P. T. Orr, Cellular microcystin content in N-limited *Microcystis aeruginosa* can be predicted from growth rate, *Applied and Environmental Microbiology* **67**:pp. 278–283 2001
- [44] P. T. Orr and G. J. Jones, Relationship between microcystin production and cell division rates in nitrogen-limited *Microcystis aeruginosa* cultures, *Limnology and oceanography* **43**:pp. 1604–1614 1998
- [45] L. A. Lawton, C. Edwards, K. A. Beattie, S. Pleasance, G. J. Dear, and G. A. Codd, Isolation and characterization of microcystins from laboratory cultures and environmental samples of *Microcystis aeruginosa* and from an associated animal toxicosis, *Natural Toxins* **3**:pp. 50–57 1995
- [46] E. P. Blanco, C. Karlsson, J. Pallon, and E. Granéli, Phosphorus, *Aquatic microbial ecology* **71**:pp. 91–97 2013
- [47] J. Muñoz Sabater, ERA5-Land monthly averaged data from 1981 to present, *Copernicus Climate Change Service (C3S) Climate Data Store (CDS)* **10**: 2019

- [48] E. L. Dan, M. Dînşoreanu, and R. C. Mureşan. “Accuracy of six interpolation methods applied on pupil diameter data”. *2020 IEEE international conference on automation, quality and testing, robotics (AQTR)*. IEEE. 2020, pp. 1–5.
- [49] H. Akima, A new method of interpolation and smooth curve fitting based on local procedures, *Journal of the ACM (JACM)* **17**:pp. 589–602 1970
- [50] N. Gorelick, M. Hancher, M. Dixon, S. Ilyushchenko, D. Thau, and R. Moore, Google Earth Engine: Planetary-scale geospatial analysis for everyone, *Remote Sensing of Environment* **202**:pp. 18–27 2017
- [51] A. Government. *Pigeon Lake, Alberta - Boundary (GIS data, polygon features)*. [https://open.alberta.ca/dataset/gda-dig\\_2008\\_0828](https://open.alberta.ca/dataset/gda-dig_2008_0828). Accessed: 2024-09-10. 2020.
- [52] A. Government. *Pine Lake, Alberta - Boundary (GIS data, polygon features)*. [https://open.alberta.ca/opendata/gda-dig\\_2008\\_0829](https://open.alberta.ca/opendata/gda-dig_2008_0829). Accessed: 2024-09-10. 2020.
- [53] U. G. Survey. *USGS National Geochemical Database: Rock*. <https://www.sciencebase.gov/catalog/item/50d35261e4b062c7914ebd14>. Accessed: 2024-09-10.
- [54] C. J. G. Loewen, F. R. Wyatt, C. A. Mortimer, R. D. Vinebrooke, and R. W. Zurawell, Multiscale drivers of phytoplankton communities in north-temperate lakes, *Ecol. Appl.* **30**:e02102 2020
- [55] R. Storn and K. Price, Differential evolution—a simple and efficient heuristic for global optimization over continuous spaces, *Journal of global optimization* **11**:pp. 341–359 1997
- [56] I. M. Sobol, Global sensitivity indices for nonlinear mathematical models and their Monte Carlo estimates, *Mathematics and computers in simulation* **55**:pp. 271–280 2001
- [57] J. Herman, W. Usher, and B. Benham, SALib: An open-source Python library for sensitivity analysis, *Journal of Open Source Software* **2**:p. 97 2017